AD-A058 355 INSTITUTE FOR DEFENSE ANALYSES ARLINGTON VA SCIENCE A--ETC F/G 17/5
SPECKLE AND SPECULAR EFFECTS IN ACTIVE INFRARED AND SUBMILLIMET--ETC(U)
JUN 78 V J CORCORAN DAHC15-73-C-0200
UNCLASSIFIED P-1294 IDA/HQ-77-19733 NL

1 OF 1
AD A058 355

END
DATE FILMED
10-78
DDC

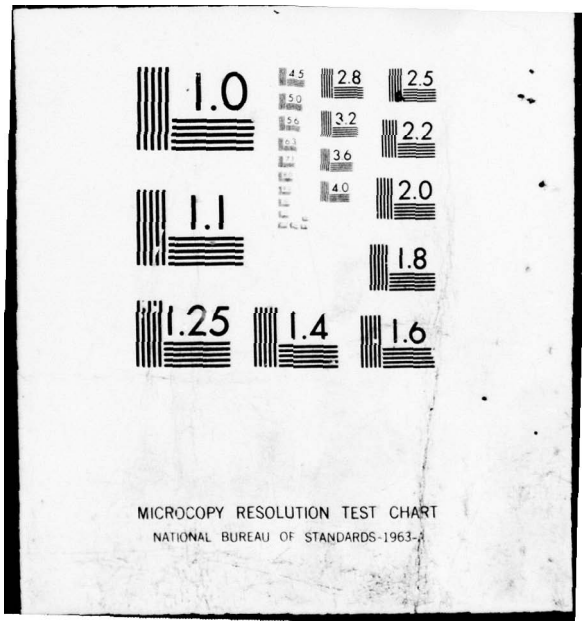
1.0
1.1
1.25
1.4
1.6
1.8
2.0
2.2
2.5
2.8
3.2
3.6
4.0
4.5
5.0
5.6
MICROCOPY RESOLUTION TEST CHART
NATIONAL BUREAU OF STANDARDS-1963-A

(12)

IDA PAPER P-1294

LEVEL II

SPECKLE AND SPECULAR EFFECTS IN ACTIVE INFRARED AND SUBMILLIMETER IMAGING SYSTEMS

Vincent J. Corcoran

June 1978

Prepared for

Office of the Under Secretary of Defense for Research and Engineering

INSTITUTE FOR DEFENSE ANALYSES
SCIENCE AND TECHNOLOGY DIVISION

IDA Log No. HQ 77-19733

The work reported in this document was conducted under contract DAHC15 73 C 0200 for the Department of Defense. The publication of this IDA Paper does not indicate endorsement by the Department of Defense, nor should the contents be construed as reflecting the official position of that agency.

UNCLASSIFIED

SECURITY CLASSIFICATION OF THIS PAGE (When Data Entered)

REPORT DOCUMENTATION PAGE	READ INSTRUCTIONS BEFORE COMPLETING FORM
1. REPORT NUMBER (14) P-1294	2. GOVT ACCESSION NO. / 3. RECIPIENT'S CATALOG NUMBER (9)
4. TITLE (and Subtitle) (6) Speckle and Specular Effects in Active Infrared and Submillimeter Imaging Systems.	5. TYPE OF REPORT & PERIOD COVERED Final rept.
	6. PERFORMING ORG. REPORT NUMBER P-1294
7. AUTHOR(s) (10) Vincent J. Corcoran	8. CONTRACT OR GRANT NUMBER(s) (15) DAHC 15-73-C-0200
9. PERFORMING ORGANIZATION NAME AND ADDRESS Institute for Defense Analyses 400 Army-Navy Drive Arlington, Virginia 22202	10. PROGRAM ELEMENT, PROJECT, TASK AREA & WORK UNIT NUMBERS Task T-136
11. CONTROLLING OFFICE NAME AND ADDRESS Defense Advanced Research Projects Agency 1400 Wilson Boulevard Arlington, Virginia 22209	12. REPORT DATE (11) June 1978
	13. NUMBER OF PAGES 98
14. MONITORING AGENCY NAME & ADDRESS (if different from Controlling Office) DUSD (R&AT) The Pentagon Washington, D.C. 20301 (12) 93p.	15. SECURITY CLASS (of this report) UNCLASSIFIED
	15a. DECLASSIFICATION DOWNGRADING SCHEDULE N/A

16. DISTRIBUTION STATEMENT (of this Report)

Approved for public release; distribution unlimited.

17. DISTRIBUTION STATEMENT (of the abstract entered in Block 20, if different from Report)

N/A (18) IDA/HQ, SBIE

DDC RECEIVED SEP 1 1978 B

18. SUPPLEMENTARY NOTES

N/A (19) 77-19733, AD-E500 030

19. KEY WORDS (Continue on reverse side if necessary and identify by block number)

speckle, specular reflection, infrared images, submillimeter waves, images, identification, recognition, surface roughness, scattering

20. ABSTRACT (Continue on reverse side if necessary and identify by block number)

Speckle effects and specular reflections from nondiffuse surfaces affect the ability of active infrared and submillimeter systems to image scenes. These effects and associated problems with respect to recognition and identification of images are investigated in this report.

DD FORM 1 JAN 73 1473 EDITION OF 1 NOV 65 IS OBSOLETE

UNCLASSIFIED

SECURITY CLASSIFICATION OF THIS PAGE (When Data Entered)

403 108 LB

IDA PAPER P-1294

SPECKLE AND SPECULAR EFFECTS IN ACTIVE INFRARED AND SUBMILLIMETER IMAGING SYSTEMS

Vincent J. Corcoran

June 1978

INSTITUTE FOR DEFENSE ANALYSES
SCIENCE AND TECHNOLOGY DIVISION
400 Army-Navy Drive, Arlington, Virginia 22202

Contract DAHC15 73 C 0200
Task T-136

ABSTRACT

Speckle effects and specular reflections from nondiffuse surfaces affect the ability of active infrared and submillimeter systems to image scenes. These effects and associated problems with respect to recognition and identification of images are investigated in this paper.

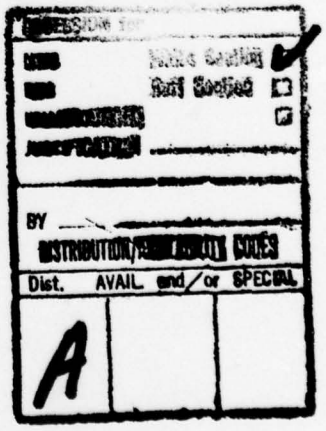

ACKNOWLEDGMENTS

The author thanks the following authors and publishers for their permission to reproduce figures from their publications in this paper:

- Mark J. Beran and George B. Parrent, Jr., authors of *Theory of Partial Coherence*, published by Prentice-hall, Inc.
- McGraw-Hill Book Company, Inc., publishers of *Introduction to Fourier Optics*, by Joseph W. Goodman
- Optical Society of America, publishers of *Optics News*, in which the article "Speckle," by Nicholas George, appeared
- Springer-Verlag, publishers of *Laser Speckle and Related Phenomena*, edited by J. C. Dainty.

CONTENTS

SUMMARY

Long-wavelength imaging systems are of interest for improved imaging capability under adverse weather conditions. Active imaging systems have been proposed in the far-infrared and submillimeter spectral regions as possibly superior to passive imaging devices. A previous paper, IDA Paper P-1163 (Ref. 1), quantitively analyzed laser-aided FLIR systems requirements on lasers based on diffuse surfaces and indicated problems associated with speckle and specular effects. This paper extends the analysis of speckle and specular effects and considers ways of reducing these effects, which are peculiar to illuminators that are highly coherent.

The analyses have produced the following results:

1. The general expression for coherent active imaging, including scene information, surface roughness, turbulence, and optics, has been derived.
2. A single expression for the speckle and specular components due to scattering from a rough surface has been obtained, and computer plots of the scattering diagrams, peak values, angular bandwidth, and relative integrated values have been determined. The equations and the plots determine the modification to the range equation that must be made to account for specular and speckle effects.
3. The correlation function for the speckle pattern has been obtained, and computer plots for various surfaces have been made.

4. The turbulence effect due to nonuniform variations in the index of refraction are expected to be negligible in the far-infrared and submillimeter regions for ranges less than 5 km; however, turbulence due to the nonuniform absorption may become significant at longer wavelengths.

5. The influence of optics has been considered, and the analysis indicates that a small-f/number system must be used in order to reduce the speckle effects.

6. Speckle reduction techniques have been considered, including the following generic techniques:

   - Decrease in spatial coherence
   - Decrease in temporal coherence
   - Aperture integration
   - Temporal integration.

   Of the various specific techniques considered, aperture integration and frame-to-frame or time delay and integration appear to be most promising.

7. Specular component reduction using nonlinear electronic processing techniques has been considered. These techniques essentially limit the peak values of the signal to suppress the specular component relative to other components.

As a result of these analyses, it is concluded that active imaging in the far-infrared and submillimeter regions is a difficult task, and a number of problems must be solved before active long-wavelength imaging can be considered a viable approach to adverse-weather imaging requirements.

I. INTRODUCTION

Single-element line scanners and scanned arrays of detectors as employed in FLIRs have been used for infrared imaging for a number of years. Recently, research and development began on focal-plane arrays in the infrared region. Consideration has also been given to using lasers for illuminators with these systems.

An active system that scans a scene with a laser boresighted to a scanning receiver is under investigation for imaging in inclement weather (Ref. 2). In this case, the submillimeter region has been chosen as a compromise between the far-infrared wavelengths, where satisfactory resolution can be obtained, and the millimeter region, where good atmospheric transmission can be obtained.

Imaging implies the ability of the observer to recognize and/or classify objects in a scene (Ref. 3). One of the factors that limits the usefulness of the image of a scene, in addition to an unsatisfactory signal level, is the resolution of the system relative to the size of the objects of interest in the scene.

Speckle effects caused by the coherent illumination of rough surfaces and specular reflections from non-diffuse surfaces also affect the ability of submillimeter systems to produce useable images of illuminated scenes.

Laser speckle has been studied since the first visible CW laser was demonstrated (Ref. 4). Considerable work has been done on the statistical properties of the speckle in the observation plane. Some work has related the results in the observation plane to the reflecting surface under the assumption that

the statistical deviations from the mean of the radiation in the speckle pattern in the observation plane obey Gaussian statistics and the correlation distance on the reflecting surface is zero; i.e., the surface consists of zero-width deviations that can deviate an infinite amount from the mean (Ref. 5). Less work has been devoted to studying less restrictive approximations to the problem of determining the characteristics of radiation reflected from rough surfaces. Even in these studies, the approximations have been somewhat idealized (Ref. 6).

Methods for reducing speckle have also been studied (Ref. 7). The generic techniques for decreasing speckle include spatial and temporal reduction of coherence, aperture integration with the aperture considerably larger than the speckle size, and time averaging with a moving aperture.

In the far-infrared and submillimeter regions, the surfaces of most man-made objects are usually not very rough relative to the wavelength of the illuminating radiation. In fact, a surface often consists of a composite of a number of smooth surfaces. The properties of the speckle pattern, therefore, can be expected to be different from those caused by a very rough surface, and specular effects must be included. In an imaging system, the image quality is important, not the statistics of the radiation incident in the image plane, unless the statistics provide an evaluation of the image.

An active infrared or submillimeter imager might be a single-detector-element line scanner, a scanning array of detectors (either parallel or serial), or a mosaic (e.g., charge-coupled device, charge injection device). Some important questions to be answered with respect to the image are: (1) what is the output of the imaging system, (2) is the image satisfactory, and (3) what can be done to improve the image? The answers to these questions partially depend upon speckle and specular effects.

A previous paper, IDA Paper P-1163 (Ref. 1), quantitatively analyzed laser-aided FLIR systems requirements on lasers based on diffuse surfaces and indicated problems associated with speckle and specular effects. This paper extends the analysis of speckle and specular effects and considers ways of reducing these effects, which are peculiar to illuminators that are highly coherent.

In this paper the general expression for the output current of an imaging detector is determined as a function of the scene information, the roughness of the reflecting surfaces in the scene, the atmospheric turbulence, and the optics of the receiver. Specific expressions for speckle and specular effects are obtained in the Fresnel region and Fraunhofer region or far field. Calculations are made for the mean intensity and mutual intensity in the far field to determine the effect of the roughness on the speckle and specular components. The effects of turbulence and optics are considered. Methods for reducing speckle and specular effects are treated.

In particular, the relative value of the speckle to the specular component reflected from a surface as a function of angle is calculated. Also, the spatially integrated value of the speckle and the specular component are determined. This information is needed to determine the signal level of the speckle image or the amount of energy in the specular return.

The correlation function of the output current is determined as a function of the spatial distance. This gives an indication of the effect of the roughness on the system resolution, since the minimum spot size is related to the spatial correlation.

Whereas other papers have limited the types of surface roughness considered, all variations of roughness and correlation lengths for a Gaussian surface are treated in this paper.

The analysis in this paper is limited to two dimensions; however, the extension to three dimensions is obvious in rec-

tangular coordinates. If cylindrical coordinates are used in the three-dimensional analysis, Bessel functions replace the sinusoidal functions, but the basic results are essentially the same. Also, a perfectly polarized pattern is assumed. The extension to partially polarized patterns is evident (Ref. 5).

Although a general expression is derived from which a variety of calculations can be made, only far-field calculations for an envelope detection system are made in this paper. The extension of the analysis to heterodyne detection can be made with the use of the general equation. The transition from calculations using the Fraunhofer type of expressions obtained in the far field to the calculations with the expression derived for the Fresnel region should be straightforward. The second-order statistics studied in this paper can be identified as a means to determine the resolution capabilities. Each of these problems is expected to be addressed in future tasks.

II. ANALYSIS

A. BACKGROUND

Before proceeding with the analysis, some background comments on speckle and specular effects will be made. A more detailed summary treatment of speckle is contained in Appendix A.

Figure 1 is a picture of laser speckle caused by constructive and destructive interference in the observation plane due to the superposition of electric fields propagated from an illuminated rough surface as illustrated in Fig. 2. When a lens is inserted before the observation plane, the size of the speckle spots caused by the rough surface are essentially the same as the Airy disc for the lens. Figure 3a shows the specular effect when the observer is close to the reflection angle of a smooth surface, and Fig. 3b illustrates the problem that is encountered in situations where the surface is tilted so that the observer is not close to the reflection angle. In the case of Fig. 3b there is no observable return from the illuminated surface. In Fig. 4a the combined speckle and specular effects are shown. The specular component is located close to the center of the figure and is distorted somewhat by the speckle effects. Figure 4b illustrates the fact that averaging reduces the speckle contrast so that an Airy disc in a gray background results.

To illustrate the problem associated with active imaging systems, consider a FLIR system with CO_2 laser illumination. Figure 5a shows the image created by an active FLIR using a 10.6 μm illuminator. This figure illustrates the problem associated with active imaging at long wavelengths. Identification of the object in this figure is virtually impossible despite the

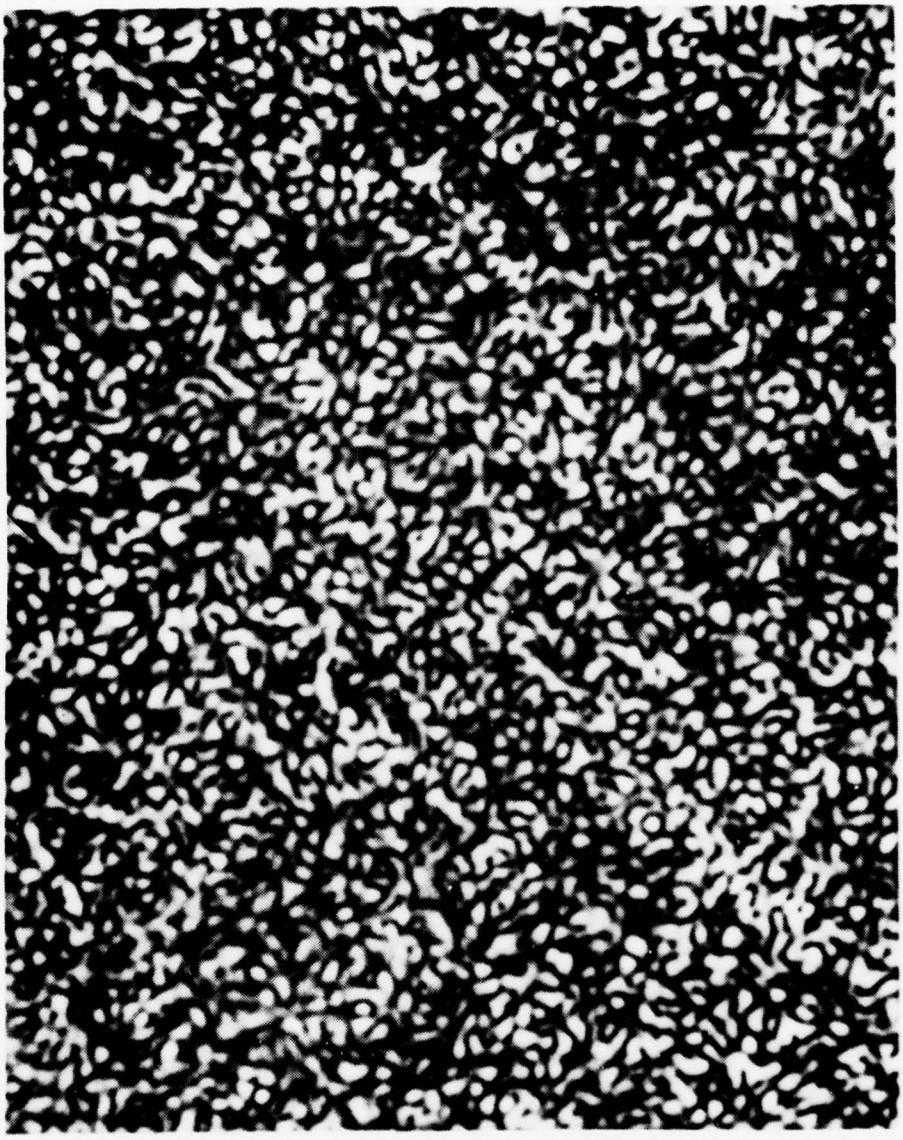

FIGURE 1. Typical speckle pattern caused by coherent superposition of electric field in the image plane after reflection of laser radiation from a very rough surface. (Source: Ref. 8)

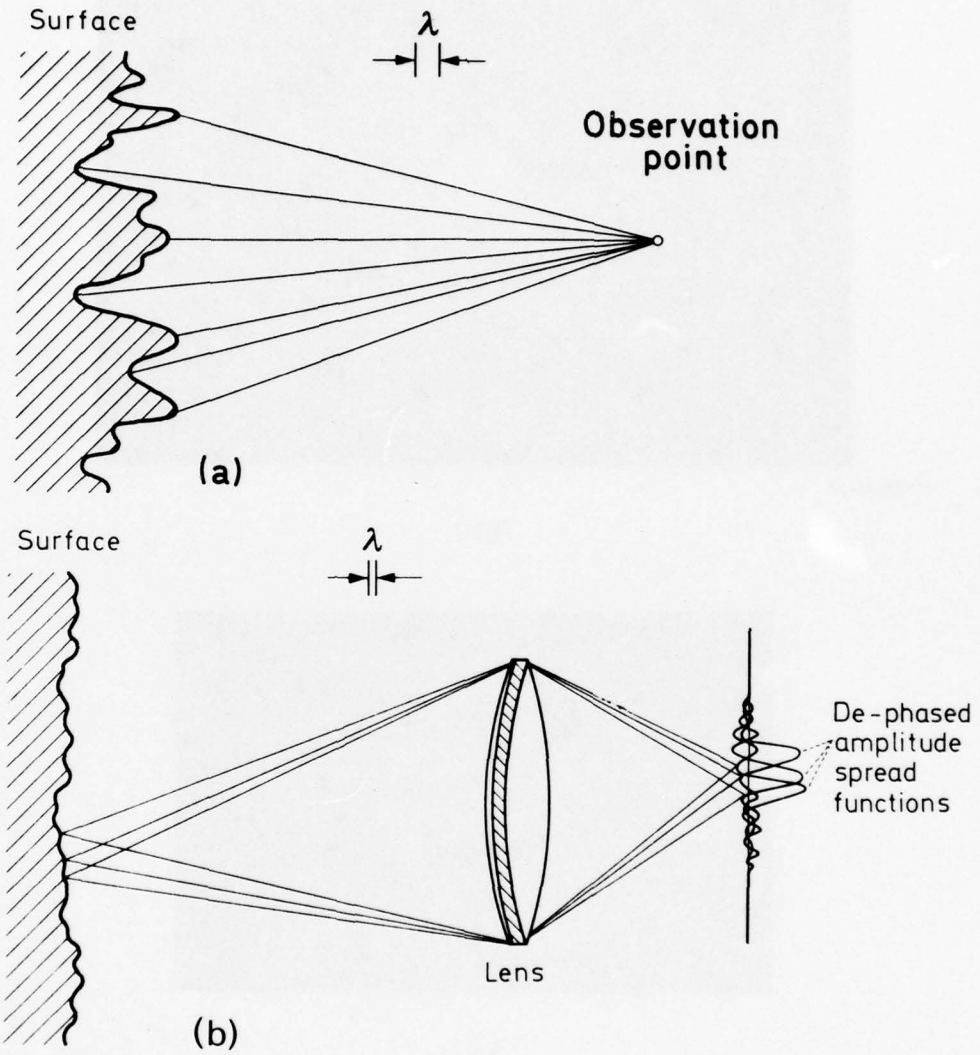

FIGURE 2. Diagram showing how speckle occurs: (a) superposition of electric fields at observation point without intervening optics; (b) superposition of fields in image plane of optics represented by a lens. In this representation, the field in the image plane is considered to be due to the summation of uncorrelated point sources on the reflecting surfaces. (Source: Ref. 5)

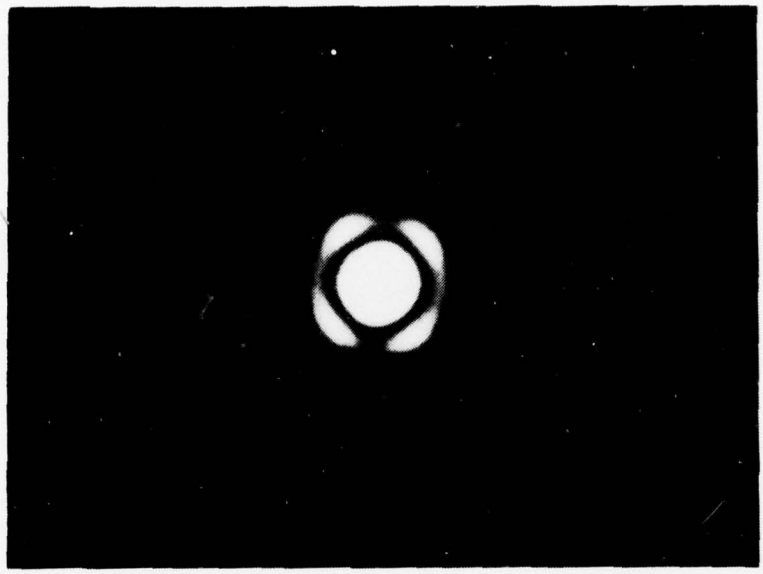

11-23-76-23

(a)

(b)

FIGURE 3. Specular pattern in the image plane caused by illuminating a smooth surface with laser radiation: (a) image close to the Fresnel reflection angle; (b) image far from the Fresnel angle, showing that virtually no radiation is contained at angles far from the Fresnel angle. [Source of (a): Ref. 9]

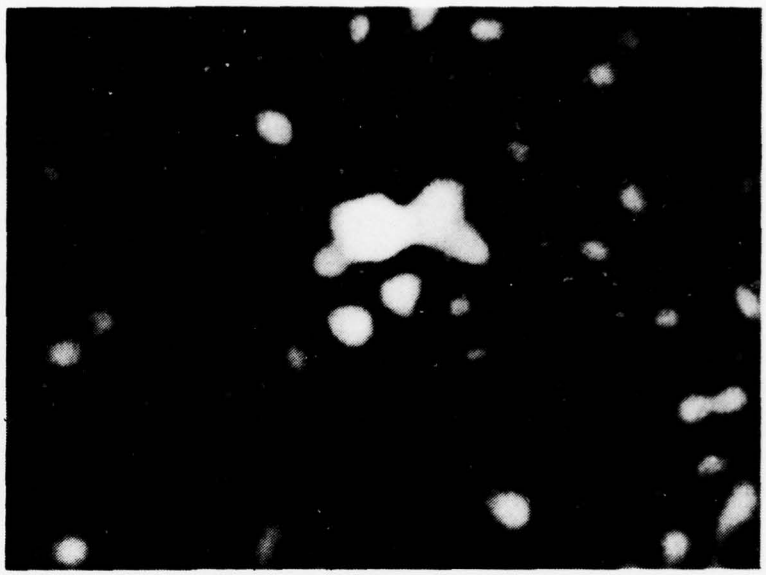

11-23-76-24

FIGURE 4a. Combined speckle and specular effects caused by reflection from slightly or moderately rough surface. (Source: Ref. 9)

11-23-76-22

FIGURE 4b. Effect of averaging speckle and specular effects by superposition of many patterns during exposure time of the photograph. (Source: Ref. 9)

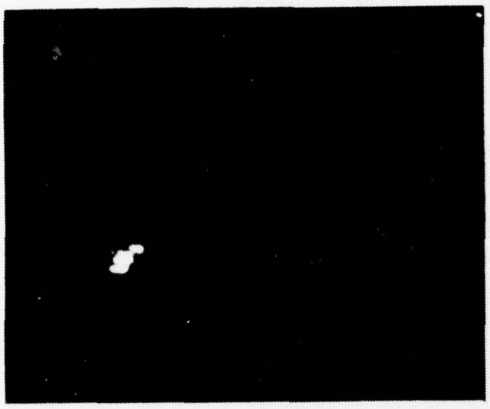

FIGURE 5a. Active FLIR image produced by illuminating a scene with 10.6 μm radiation from a CO_2 laser. (Source: Ref. 1)

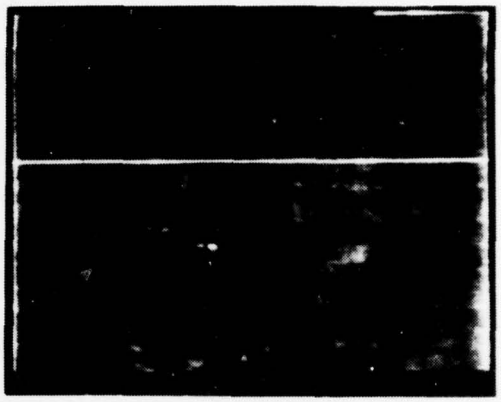

FIGURE 5b. Passive FLIR image produced by thermal radiation from scene. (Source: Ref. 1)

FIGURE 5c. Photograph of same scene with jeep located in heavy vegetation. (Source: Ref. 1)

fact that the signal return is very strong. Figure 5b shows the thermal image of the same object. Upon careful observation, a vehicle can be seen in the left center of the picture. Figure 5c is a photograph of the vehicle, which is a jeep, in heavy vegetation. Figures 5a-c illustrate the problems associated with imaging with a long-wavelength active system. It is evident that the strong return obtained by using an active system provides a cueing advantage despite the fact that the object cannot be recognized or classified.

B. IMAGING CONCEPT

The active imaging concept is illustrated in Fig. 6. A highly coherent source illuminates a scene, including an object which has a rough surface, and radiation from the object is partially scattered into a receiver, where an image of the object is to be formed. The definitions for a rough surface, relative to the wavelength of the radiation, are given in Fig. 7a, where the change from a smooth surface to a very rough surface is shown. The roughness of the surface is determined by the standard deviation of the surface deviations from the mean value of the surface relative to the wavelength. The concept of correlation length is illustrated in Fig. 7b. It is clear that two surfaces of equal roughness can have different correlation lengths. From another viewpoint, the spatial frequency spectra or power spectra of the two surfaces are different. In the upper diagram of Fig. 7b the correlation length is long or the power in the spatial frequency spectrum is confined to low-frequency components. In the lower diagram the correlation length is short, corresponding to a higher-frequency cutoff in the power spectrum.

C. GENERAL ANALYSIS, FIRST-ORDER STATISTICS

When light impinges upon a rough surface, the scattered radiation consists of a specular component and a diffuse component. The relative amounts of radiation in each depend upon

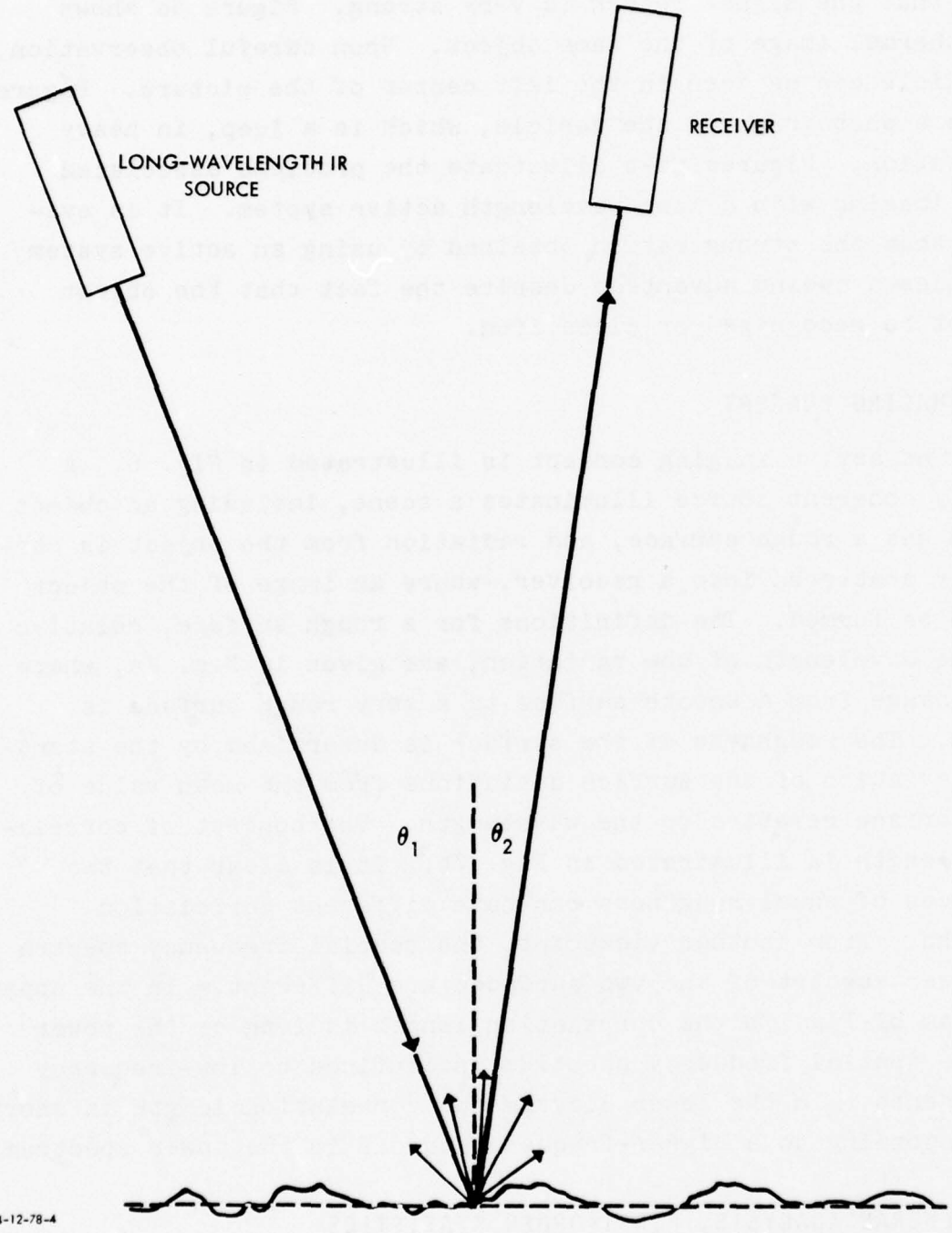

FIGURE 6. Generic active imaging concept. Diagram shows laser illuminating scene and imaging receiver.

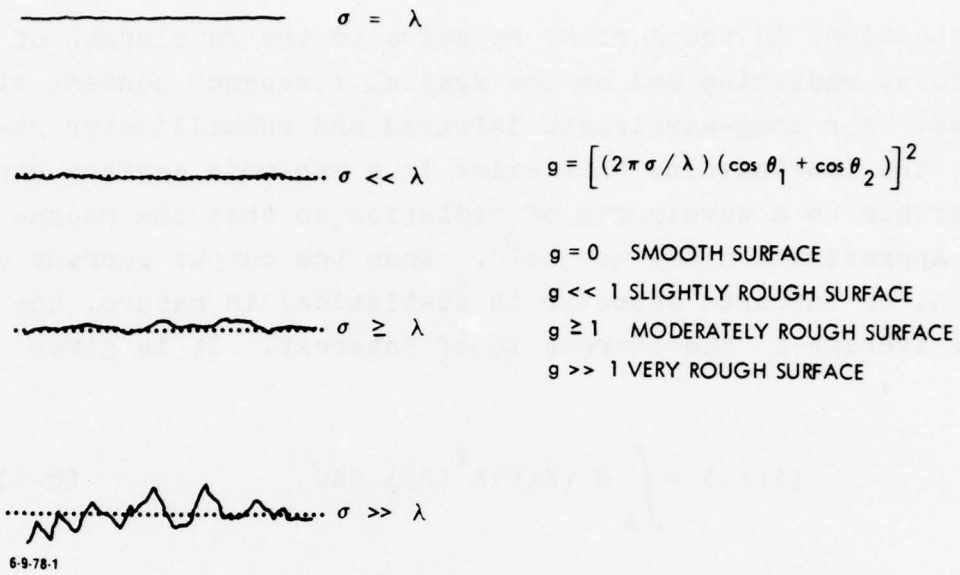

FIGURE 7a. Illustration of quantitative concept of roughness as a measure of the deviation of the surface from the mean relative to the radiation wavelength.

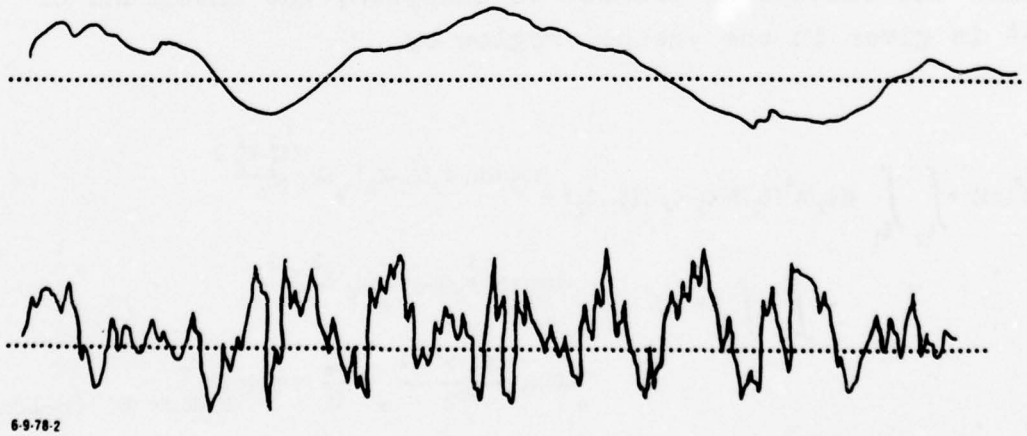

FIGURE 7b. Illustration of two surfaces with the same roughness but different correlation lengths which are related to the spatial-frequency content of the surface roughness.

the fluctuations in the surface relative to the wavelength of the incident radiation and on the spatial frequency content of the waves. For long-wavelength infrared and submillimeter radiation, the fluctuations that exist in a man-made surface can be comparable to a wavelength of radiation so that the rough-surface approximation may not hold. When the output current of an optical or infrared detector is statistical in nature, the ensemble average of the current is of interest. It is given by*

$$\langle i(t) \rangle = \int_A R \, \langle E(P) E^*(P) \rangle \, dA. \qquad \text{(B-4)}$$

With a knowledge of the spatial variation of the electric field across the detector surface, the output current for the problem of interest can be calculated from Eq. B-4. The detector output current can be found, therefore, by determining the average power in the detector plane and integrating over the detector surface.

When the conceptual problem is analyzed, the integrand of Eq. B-4 is given in the Fresnel region by

$$\langle E(\eta) E^*(\eta) \rangle = \int_{\xi_2} \int_{\xi_1} A(\xi_1) A^*(\xi_2) R(\xi_1, \xi_2) T(\xi_1, \xi_2) \, e^{ik_o \sin\theta_2 (\xi_1 - \xi_2)} \, e^{ik_o \frac{(\xi_1^2 - \xi_2^2)}{2r_o}}$$

$$\cdot \int_{y'} \int_{y} P(y) P^*(y') \, e^{-iko \sin\theta_2 (y - y')} \, e^{ik_o \frac{(y^2 - y'^2)}{2r_o}}$$

$$e^{-2ik_o \frac{(y\xi_1 - y'\xi_2)}{2r_o}} \, e^{-i \frac{2\pi}{\lambda f} (y - y')\eta} \, d\xi_1 d\xi_2 dy \, dy' \qquad \text{(B-12a)}$$

*All numbered equations in this chapter are from Appendix B, and their numbering conforms to that of Appendix B.

In the far field this reduces to

$$\langle E(\eta)E^*(\eta)\rangle = \int_{\xi_2}\int_{\xi_1} A(\xi_1)A^*(\xi_2)R(\xi_1,\xi_2)T(\xi_1,\xi_2)\; e^{ik_o \sin\theta_2(\xi_1-\xi_2)}\, d\xi_1 d\xi_2$$

$$\cdot \int_{y'}\int_{y} P(y)P^*(y')\; e^{-ik_o(\sin\theta_2+\sin\theta_f)(y-y')}\, dy dy' \qquad \text{(B-12b)}$$

where $A(\xi)$ describes the scene information

$R(\xi_1,\xi_2)$ is the statistical term corresponding to the roughness

$T(\xi_1,\xi_2)$ is the statistical term corresponding to the turbulence

and $P(y)$ is the pupil function of the receiver.

Notice that in the far field the integration over the scene is independent of the integration over the pupil function if the quadratic terms are ignored, while in the Fresnel region these integrals are coupled by the term

$$e^{-\left[2ik_o \frac{(y\xi_1 - y'\xi_2)}{2r_o}\right]} .$$

The independence of the integrals in the far field is due to the fact that in the far field the phase variations caused by the coupling term are negligible, or from another viewpoint the radiation in the y plane effectively comes from a point at ∞, so the phase variations depend only on θ_2. In either case the autocorrelation of the field in the focal plane, and therefore the mean current detector output, depends on the product of the scene information, the roughness, and the turbulence, i.e., upon

$$A(\xi_1)A^*(\xi_2)R(\xi_1,\xi_2)T(\xi_1,\xi_2) \quad .$$

Equations B-12a and B-12b can be considered to be the general two-dimensional expressions to be inserted into Eq. B-4 to determine the output current of a detector in an imaging system using one or more detectors. Equations B-12a and B-12b can easily be extended to three dimensions by including the other geometrical dimension in Eq. B-6 before proceeding. Equation B-12 can be recognized as the product of two equations that are in the form of Fourier transforms. The average output current from the detector can, therefore, be considered as a convolution of a term that describes the scene, a term that describes the surface roughness, and a term that describes the turbulence effects. This convolution is multiplied by a function describing the effect of the receiver.

From this equation it is evident that the speckle can be considered to be a muliplicative noise effect because of the fact that the roughness term is convolved with the scene term. In order to completely analyze an imaging system, therefore, this multiplicative noise must be taken into account in any signal-to-noise ratio equation.

D. ROUGHNESS ANALYSIS

If only the roughness term in Eq. B-12 is considered, then the effect of the roughness can be seen to be proportional to

$$\langle \rho(y)\, \rho^{*}(y) \rangle = \frac{F_2 F_2^{*}}{4L^2} \int_{-L}^{L} \int \chi_2(k_z, -k_z)\, e^{ik_x(\xi_1 - \xi_2)}\, d\xi_1 d\xi_2 \,, \quad \text{(B-15)}$$

where $\langle \rho\rho^{*} \rangle$ is the normalized mean square field and χ_2 is the characteristic function of the surface statistics which describe the roughness. For a Gaussian surface with a correlation function of the form $\exp(-\tau^2/T^2)$, one obtains

$$\langle \rho\rho^{*} \rangle = F^2 e^{-g} \left(\rho\rho^2 + \frac{\sqrt{\pi}T}{2L} \sum_{m=1}^{\infty} \frac{g^m}{m!\sqrt{m}}\, e^{-k_x^2 T^2/4m} \right), \quad \text{(B-25)}$$

where

$$F = \sec \theta_1 \frac{1 + \cos (\theta_1 + \theta_2)}{\cos \theta_1 + \cos \theta_2}$$

$$g = [2\pi \frac{c}{\lambda}(\cos \theta_1 + \cos \theta_2)]^2$$

$$\rho_o = \frac{\sin k_x L}{k_x L}$$

$$k_x = \frac{2\pi}{\lambda} (\sin \theta_1 - \sin \theta_2)$$

θ_1 is the angle of incidence

θ_2 is the scattering angle which is measured in the opposite sense from θ_1

L is the length of the surface

T is the correlation length of the surface.

Equation B-25, which is derived from a more restrictive approach than in Ref. 10, is limited by the following conditions:

- The surface is perfectly conducting
- Shadowing and multiple scattering may be neglected
- The incident wave is plane and linearly polarized with the E vector either in the plane of incidences, xz, or perpendicular to it
- The observation point is in the far field
- The radius of curvature of the scattering elements is greater than the wavelength of the incident radiation.

The expression for the mean current, which is related to the mean scattered power through Eq. B-4, consists of two terms. The first is a specular term that is a maximum for a smooth surface ($g = 0$), and the second is a diffuse term that is zero for a smooth surface and becomes dominant for a very rough surface ($g > 1$). The specular term is highly directional, as would be

expected for the reflection from a smooth surface. Because of conservation of energy, the increase in the specular component as the surface becomes smooth requires a corresponding decrease in the total diffuse component, which causes the speckle. In principal, therefore, a speckly image is always available if the specular component is filtered unless the surface is perfectly smooth.

When Eq. B-25 is computed for various values of roughness and correlation length, the curves in Figs. 8-11 are obtained for 100 μm radiation. Figure 8a is a scattering diagram for the case of a very rough surface ($g >> 1$) when the correlation length is small. In this case, the specular component is very small compared to the speckle component. As the correlation length is increased for the same roughness, Eq. B-25 shows that the term corresponding to the specular component is unchanged. The speckle component, however, increases in peak value, and the beamwidth of the radiation due to the speckle component decreases, as shown in Figs. 8b-d. A surface with a large correlation length might be considered to be locally smooth, thus providing a rationale for the beam's narrowing for this condition. It should also be noted that the apparent random variation for the cases where $T > \lambda$ is an artifact due to the number of points sampled by the computer. Actually, the detail of the sidelobes looks more like Fig. 11.

For Fig. 9a the surface is moderately rough ($g \geq 1$), and the specular component increases relative to the speckle component. In Figs. 9b-d the effect of changing the correlation length is shown. As the correlation length increases, the peak of the speckle component increases, and the beamwidth decreases as for the very rough surface.

In Fig. 10a the surface is slightly rough ($g << 1$), in which case the specular component is very large relative to the speckle compinent. Figures 10b-d show the effect of changing the correlation length. Again, the peak of speckle increases, and the beamwidth decreases as the correlation length increases.

In Fig. 11 the curve for a smooth surface ($g = 0$) is plotted. In this case there is only a specular term, which is the familiar

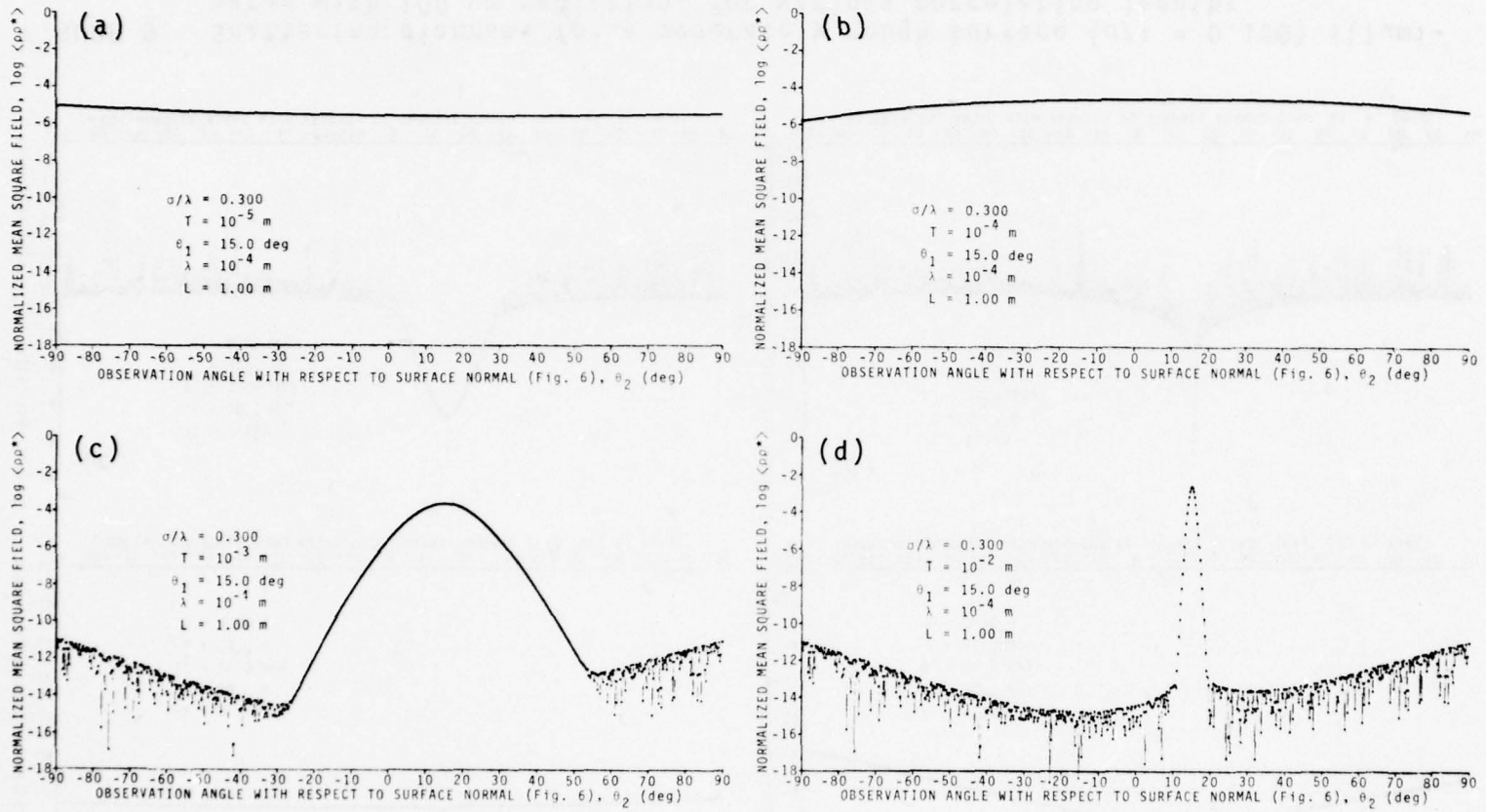

FIGURE 8. Scattering diagrams for a very rough surface ($\sigma/\lambda = 0.300$) illuminated with 100 μm radiation, for various correlation lengths.

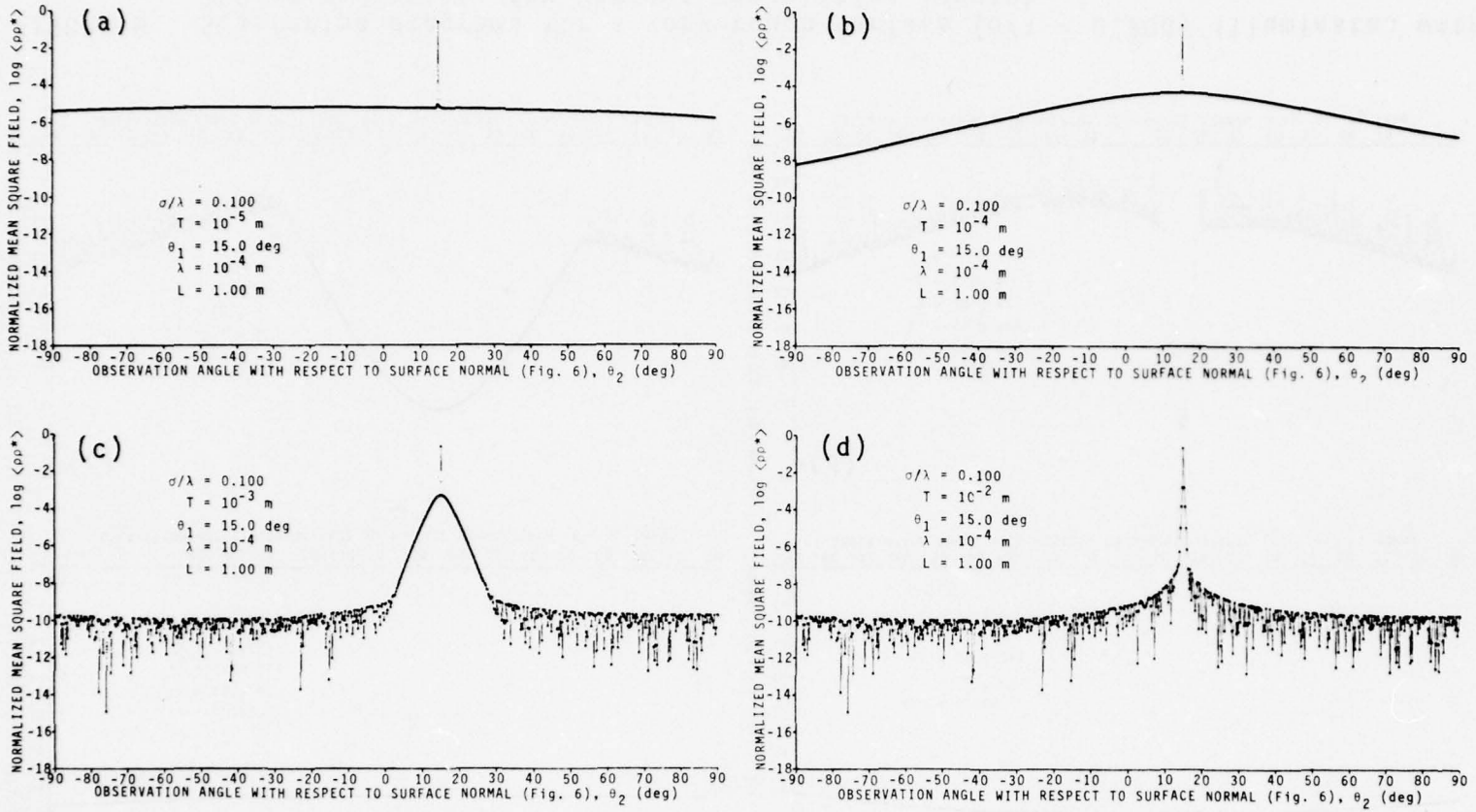

FIGURE 9. Scattering diagrams for a moderately rough surface ($\sigma/\lambda = 0.100$) illuminated with 100 μm radiation, for various correlation lengths.

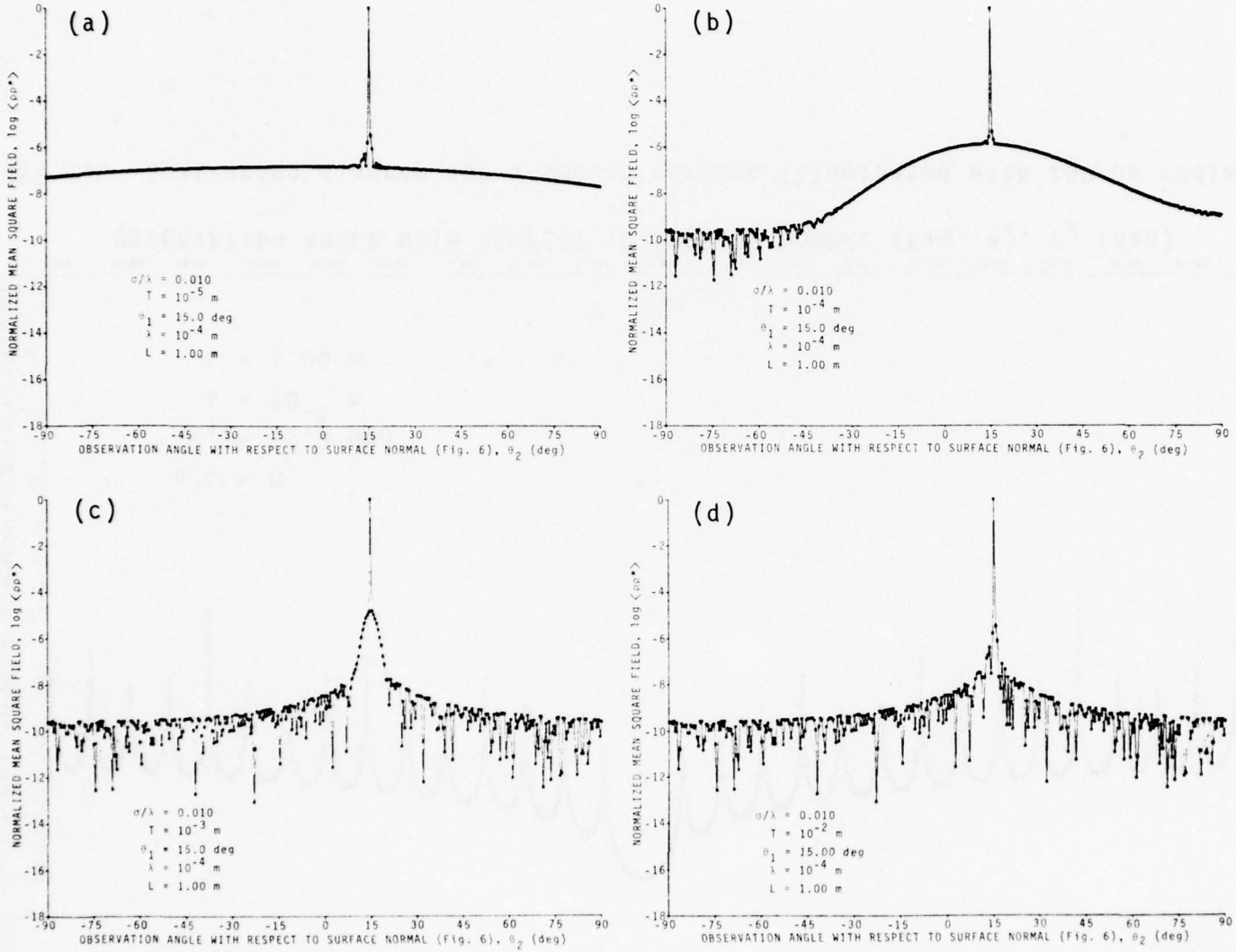

FIGURE 10. Scattering diagrams for a slightly rough surface ($\sigma/\lambda = 0.010$) illuminated with 100 μm radiation, for various correlation lengths.

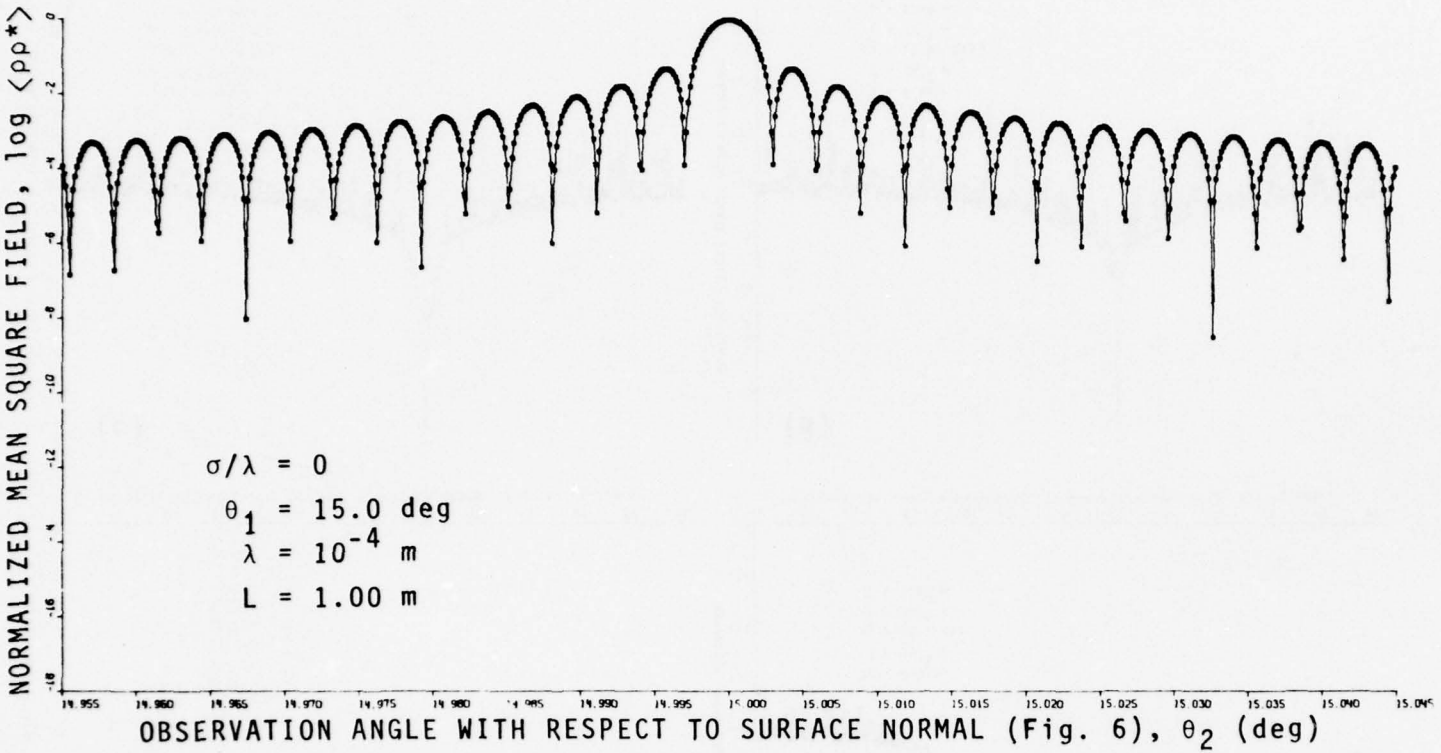

FIGURE 11. Scattering diagram for a smooth surface illuminated with 100 μm radiation.

$\sin^2 x/x^2$ term. Note that the abscissa scale of Fig. 11 is expanded over those of Figs. 8-10.

These curves are plotted in a different manner in Fig. 12 to show the change in the speckle and specular components as the roughness is varied for a fixed correlation length. As can be seen, the specular component of the radiation has a significant component for surfaces where $\sigma < \lambda/4$ and the correlation length is comparable to the wavelength of the radiation.

Similar curves are obtained for other wavelengths. For example, a computer run corresponding to Fig. 12 for 10 μm radiation is shown in Fig. 13 with the correlation length 10 times the wavelength. The similarity to Fig. 12 is evident.

Figure 14 is a plot of the ratio of the peak value of the specular component to the peak value of the speckle component for various values of roughness and various correlation lengths. It is evident that as the roughness increases, the specular component decreases relative to the speckle component in all cases. As the correlation length increases for a given value of roughness, the ratio decreases or the peak speckle component increases. The limiting case for this curve would be the case where $T \to 0$, in which case only the specular component exists.

Figure 15 shows the ratio of the speckle component relative to the sum of the speckle and specular components. This figure again shows that as the roughness increases, the value for the speckle component increases relative to the total of the two components. The results shown in Fig. 15 must be factored into the range equation to indicate the decrease in system range capability when the speckle component of the return signal is used for imaging. If the specular component could be used for imaging, the range capabilities of imaging systems would have a probability of operating at a greater or lesser range than that computed from the speckle component. The ranging capability for the specular component would be a function of the orientation of the target. Whether the return would permit identification and classification, however, is doubtful for long-wavelength systems.

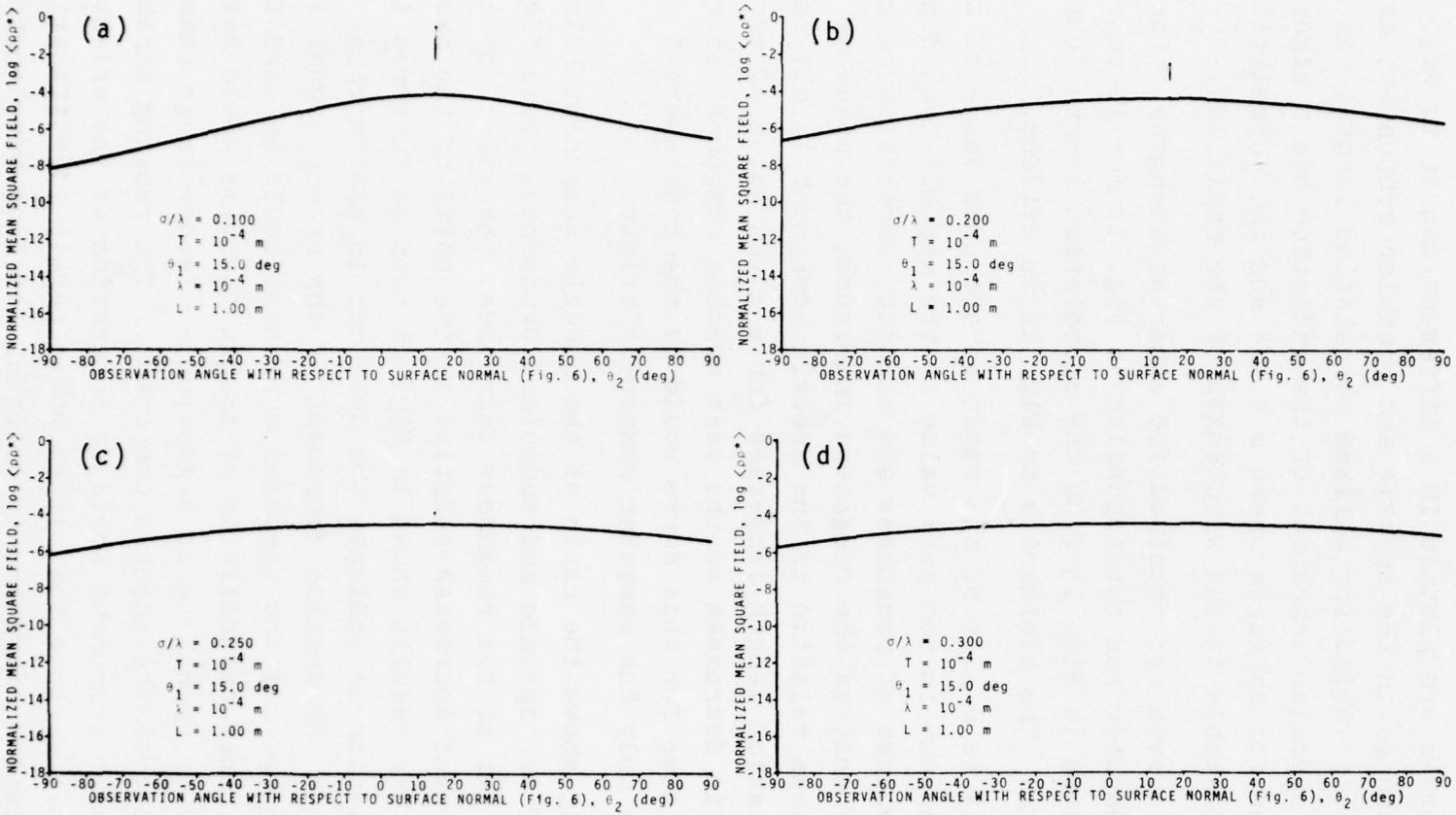

FIGURE 12. Scattering diagrams for surfaces of various roughnesses and fixed correlation length, illuminated with 100 μm radiation.

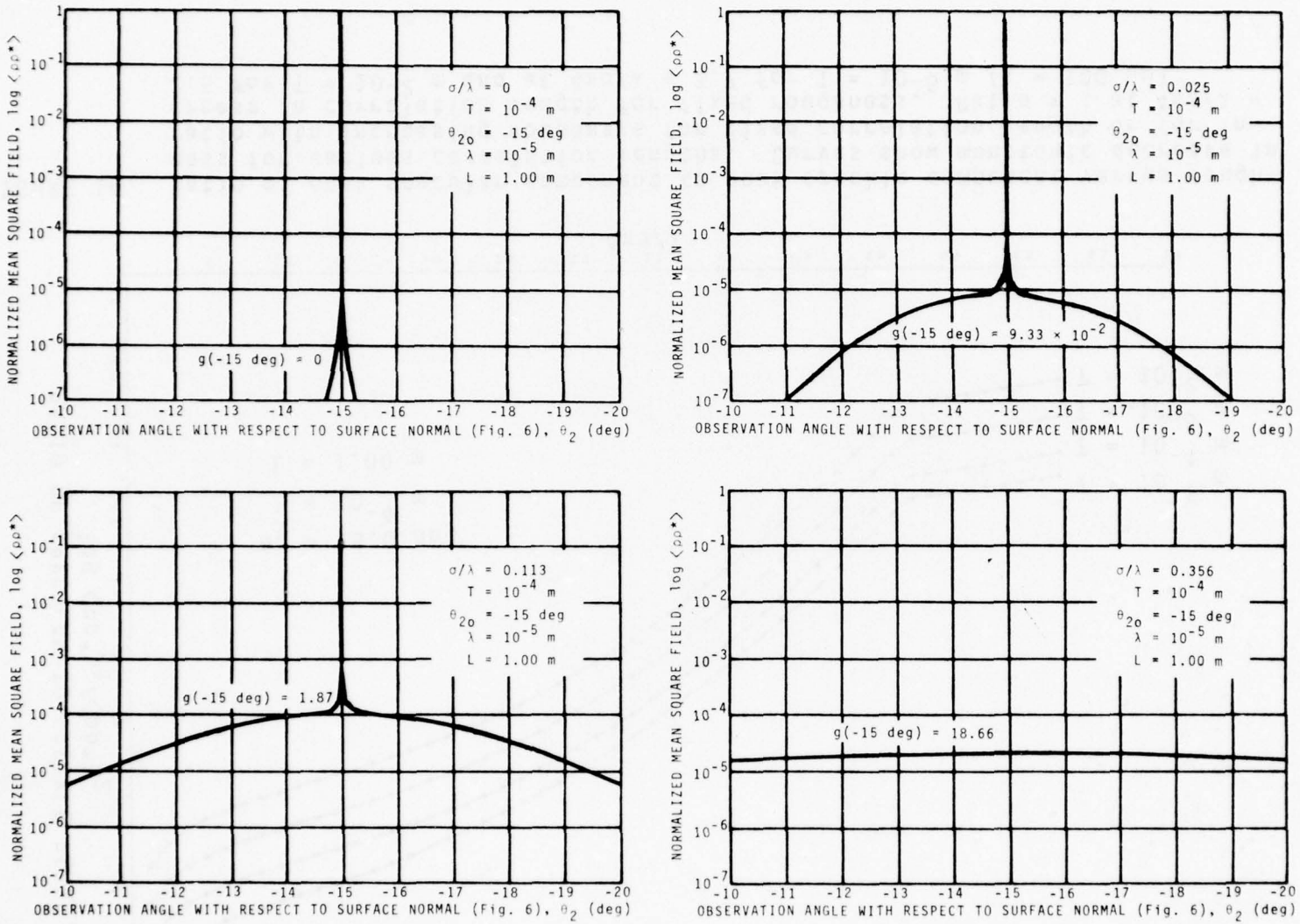

FIGURE 13. Scattering diagrams for surfaces of various roughnesses with a fixed correlation length, illuminated with 10 μm radiation. (Source: Ref. 11)

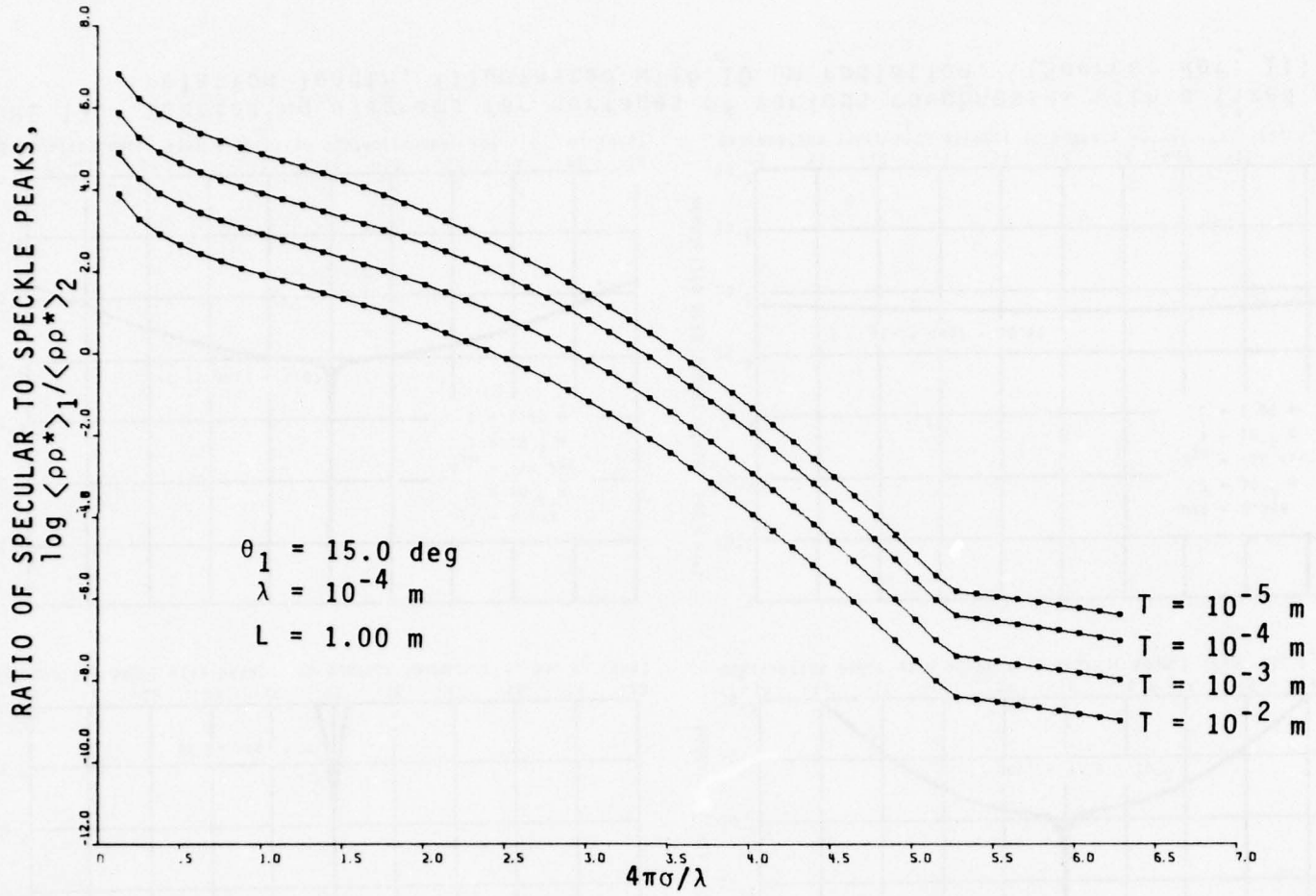

FIGURE 14. Ratio of peak specular component to peak speckle component versus roughness for various correlation lengths. Curves show monotonic decrease in ratio with increasing roughness for fixed correlation length or for increase in correlation length for fixed roughness. Ratio = 1 at $4\pi\sigma/\lambda$ = 2.5 for T = 10^{-2} m and at $4\pi\sigma/\lambda$ = 3.7 for T = 10^{-5} m (λ = 100 μm).

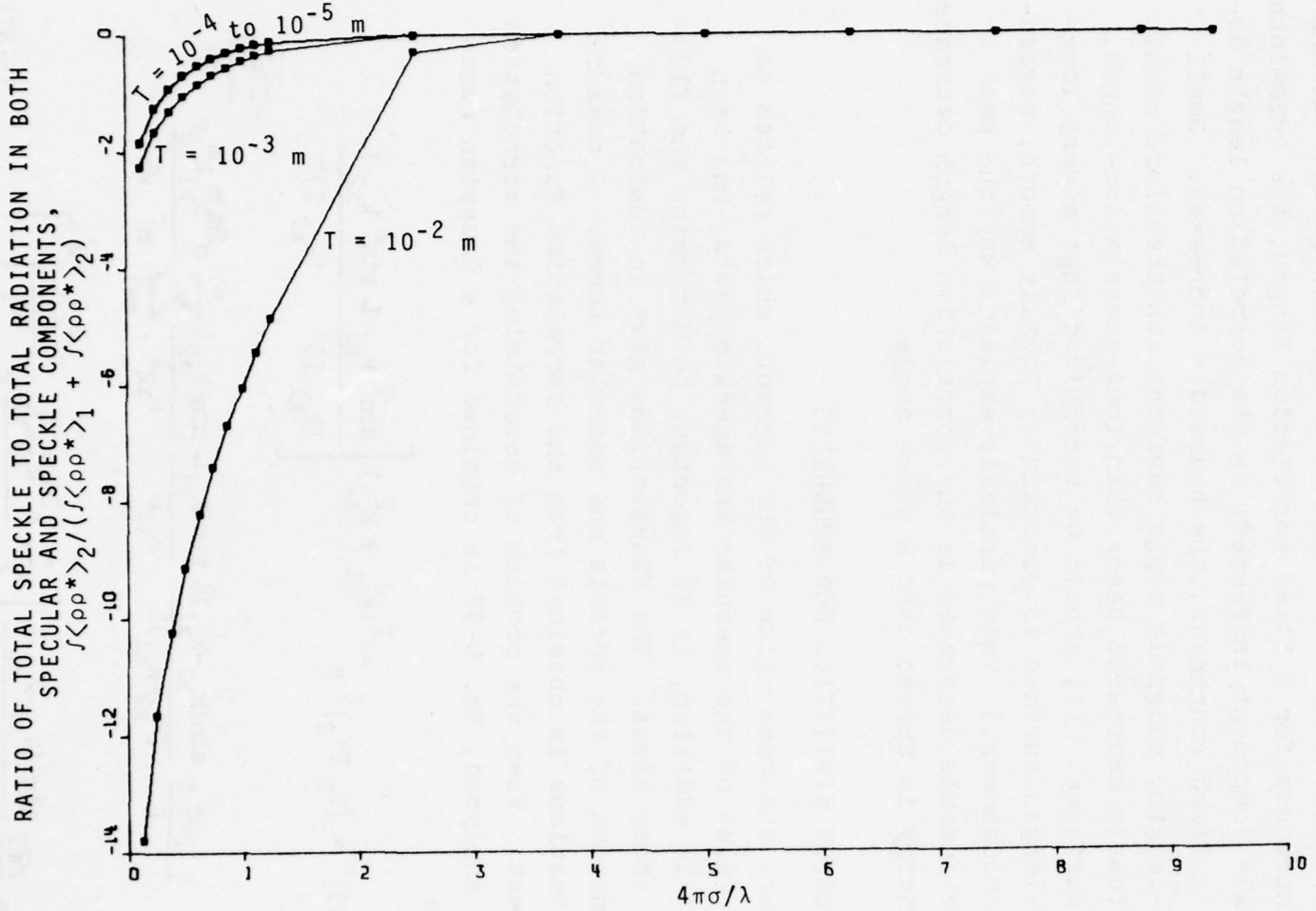

FIGURE 15. Ratios of integrated average value in speckle component to total energy versus roughness for various correlation-length curves show that for large values of roughness virtually all the energy is in the diffuse component, while for values of $\sigma/\lambda < 0.25$ significant modification to range calculations may be necessary (λ = 100 μm).

The angular beamwidth of the speckle component as a function of roughness and correlation length is shown in Fig. 16. As the roughness increases for a fixed correlation length, the beamwidth of the speckle component increases; as the correlation length decreases for a fixed roughness, the beamwidth increases. Small-correlation-length, slightly rough surfaces can therefore result in more diffusely scattered beams than long-correlation-length, very rough surfaces. (It should be recognized that a very long-correlation-length surface is essentially locally smooth, regardless of the roughness.) This partially explains why the peak value of the speckle decreases as the correlation length decreases, since the energy is spread over a wider angle.

E. SECOND-ORDER STATISTICS FOR ROUGHNESS

Thus far, the mean value of the current, which related to the average value of the specular and speckle parts, has been considered. In addition, it is important to determine the fluctuations in these terms. The fluctuations give an indication of the dimensions of the speckle and specular terms. A measure of the fluctuations is obtained from the correlation function of the current. When the problem of determining the correlation function is analyzed, Eq. B-37 is obtained for a Gaussian function. It is

$$|\langle E(P_1)\, E^*(P_2)\rangle|^2 = |F_2\, F'_2|^2\, e^{-\sigma^2(k_{z1}^2 + k_{z2}^2)} \left[\frac{\sin^2 k_{x1} L}{(k_{x1} L)^2} \frac{\sin^2 k_{x2} L}{(k_{x2} L)^2} \right.$$

$$+ \frac{2\sqrt{\pi}\, T}{L} \frac{\sin(k_{x2}-k_{x1})L}{(k_{x2}-k_{x1})L} \frac{\sin k_{x1} L}{k_{x1} L} \frac{\sin k_{x2} L}{k_{x2} L} \sum_{m=1}^{\infty} \frac{\sigma^{2m} k_{z1}^m k_{z2}^m}{m!\ \sqrt{m}} e^{\frac{-T^2 k_{x2}^2}{4m}}$$

$$\left. + \frac{\sqrt{\pi} T}{L} \frac{\sin^2(k_{x2}-k_{x1})L}{[(k_{x2}-k_{x1} L]^2} \left| \sum_{m=1}^{\infty} \frac{\sigma^{2m} k_{z1}^m k_{z2}^m}{m!\ \sqrt{m}} e^{\frac{-T^2 k_{x2}^2}{4m}} \right|^2 \right] \qquad \text{(B-37)}$$

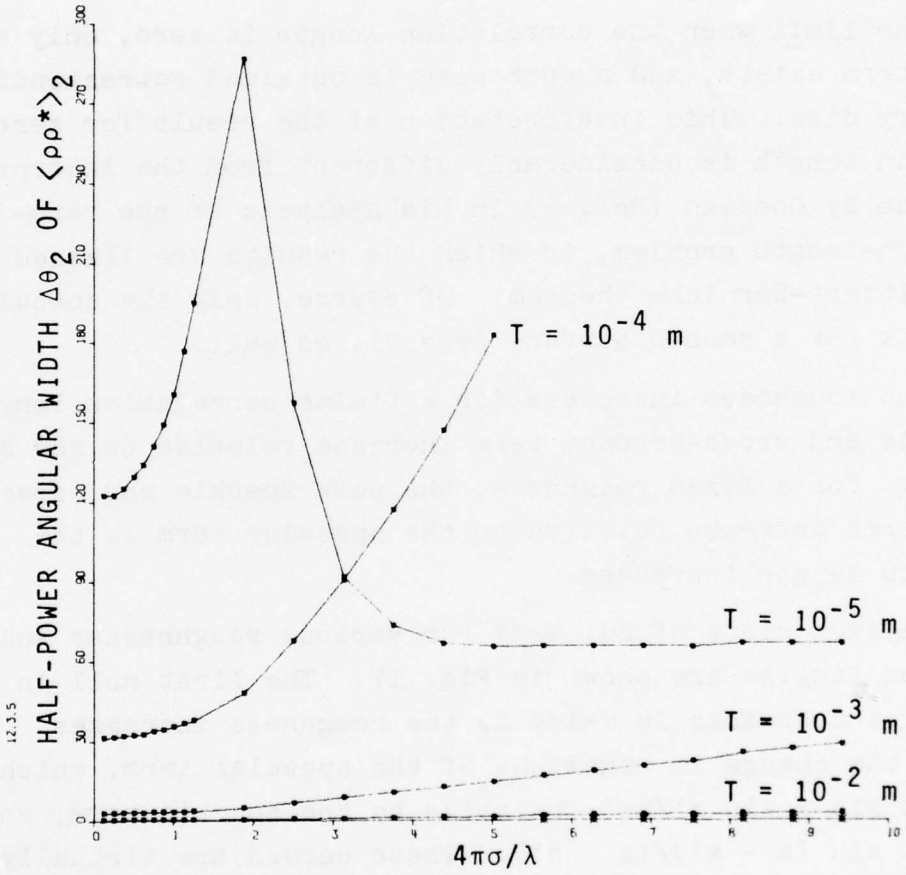

FIGURE 16. Beamwidth of speckle component versus roughness for various correlation lengths.

Equation B-37 consists of a term that is exclusively due to the speckle component and a term that is exclusively due to the specular component. It also contains a cross-product term that depends on both the speckle and specular effects. Again, the specular term depends on the roughness and wavelength, and the speckle term and the cross-product term are functions of the roughness and the correlation length.

In the limit when the correlation length is zero, only the specular term exists, and a spot size is obtained corresponding to the Airy disc. This interpretation of the result for zero correlation length is considerably different from the interpretation made by Goodman (Ref. 5) in his analysis of the zero-correlation-length problem, in which the results are likened to the Van Cittert-Zernicke theorem. Of course, only the specular term exists for a smooth surface ($\sigma = 0$), as well.

As the roughness increases for a finite correlation length, the speckle and cross-product term increase relative to the specular term. For a fixed roughness, the peak speckle and cross-product terms increase relative to the specular term as the correlation length increases.

Normalized plots of Eq. B-37 for various roughnesses and correlation lengths are shown in Fig. 17. The first null in these curves decreases in value as the roughness increases. This is due to the change in magnitude of the specular term, which depends on sin x sin x'/xx', relative to the speckle term, which depends on sin $(x - x')/(x - x')$. These curves are virtually unchanged for the range of correlation values of interest. These curves give an indication of the speckle size. It is to be emphasized that it is merely an indication, since the correlation function is angular dependent and nonstationary.

F. TURBULENCE EFFECTS

Equation B-12 indicates the way in which turbulence caused by index-of-refraction inhomogeneities affects the image. Although

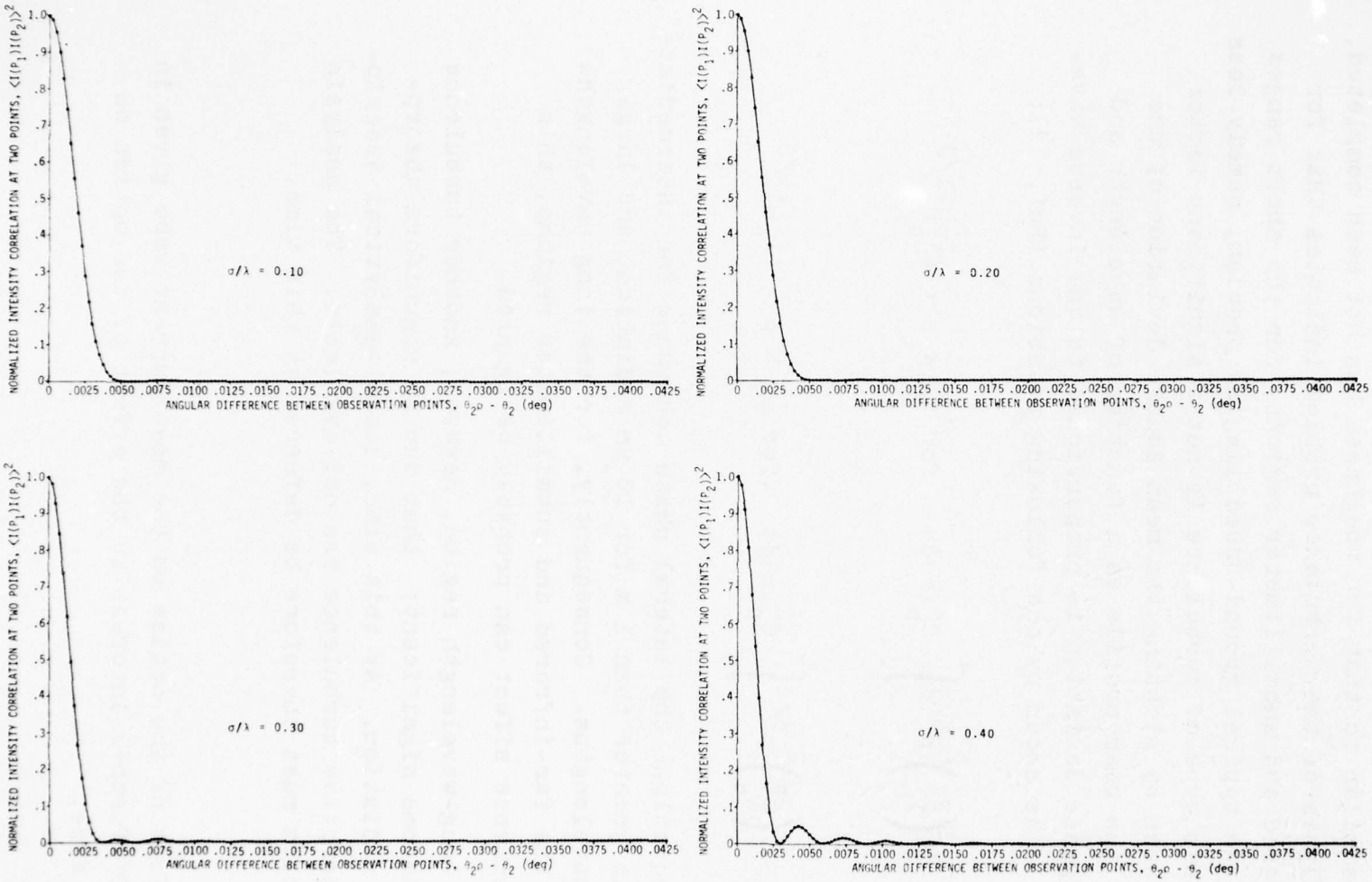

FIGURE 17. Normalized mutual intensity versus angular separation for various values of roughness. Curves show slight change in correlation angle as roughness changes.

an analysis similar to that for roughness has not been completed, previous analysis of the turbulence problem indicates that for the far-infrared and submillimeter regions, for the short ranges involved in the typical ground-based imaging problem, namely less than 5 km, this type of turbulence is not a significant factor. This can be seen by plotting the mean square deviation of the phase across the beam profile as a function of wavelength and range. The phase deviation is proportional to the inverse wavelength squared as shown by the following equations (Ref. 12):

$$\sigma_\Phi^2(\rho) = \begin{cases} 1.46\left(\frac{2\pi}{\lambda_c}\right)^2 \rho^{5/3} \int_0^L C_n^2(r)dz & \text{for } \ell_o < \rho < (\lambda_c L)^{1/2} \\ 2.91\left(\frac{2\pi}{\lambda_c}\right)^2 \rho^{5/3} \int_0^L C_n^2(r)dz & \text{for } L_o > \rho > (\lambda_c L)^{1/2} \end{cases} .$$

With these equations the lateral phase coherence for intermediate turbulence is greater than 1 m for 10 μm radiation, and larger for longer wavelengths. Consequently, for the long wavelengths involved in the far-infrared and submillimeter regions, this type of turbulence effect can probably be ignored.

In the long-wavelength region, however, another turbulence effect may become significant: that due to nonuniform absorption of the radiation. At this time, useful analytical descriptions of absorptive turbulence are not available. The analysis of this problem must therefore be deferred at this time.

G. OPTICS

The effect of the optics on the mean current were given in Eq. B-12. Of further interest is the effect of the optics on the speckle size.

The optics in the imaging system effectively take the Fourier transform of the electric field in the aperture plane. As a result, the speckle spot size for zero-correlation-distance surfaces is proportional to the wavelength and the f/number of the optics, i.e., the speckle spot diameter for zero correlation distance is

$$D_{spot} = \lambda \, f/\# \, ,$$

which is simply the resolution of the optics. The effect of optics on the visible image is illustrated in Fig. 18 for two f/number systems (Ref. 13). As can be seen from Eq. B-37, the situation is somewhat more complicated for coherent long-wavelength active systems. As the roughness, correlation length, and angle vary, the speckle spot size changes. Also, the limiting case of zero correlation distance can actually be obtained by ignoring the speckle term and considering only the specular term.

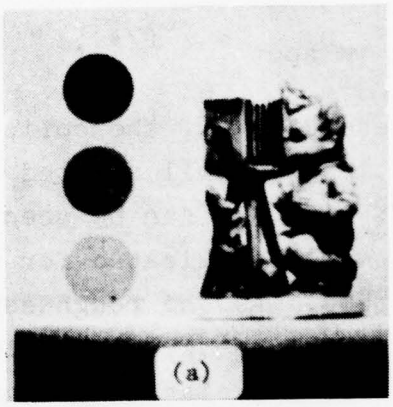

LASER
Aperture
f/8

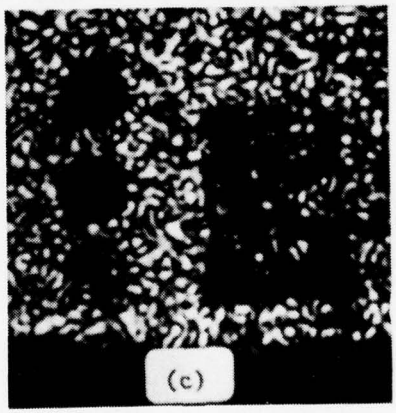

LASER
Aperture
f/190

FIGURE 18. Photographs showing change in speckle size as f/number of optics in camera is changed. (Source: Ref. 13)

III. SPECKLE REDUCTION TECHNIQUES

As has been mentioned in the introduction, a number of generic techniques can be attempted to reduce the speckle effect. These include reduction of the temporal coherence, reduction of spatial coherence, spatial averaging, and temporal averaging.

A. TEMPORAL COHERENCE REDUCTION

Decreased speckle through temporal coherence reduction can be achieved by using a multimode or multifrequency source or by frequency-modulating the source to make the transmitter essentially a noise-like source. Whereas the reduction of temporal coherence is relatively easy in the optical region, where very short wavelengths are involved and the phase change can be affected with small deviations in the frequency, temporal coherence reduction of far-infrared or submillimeter sources becomes more difficult, as indicated by the equation

$$\frac{\Delta\lambda}{\lambda} = \frac{\lambda}{\mu} \quad ,$$

which shows the change in spectral width, $\Delta\lambda$, required for a given roughness, μ, to effect a phase change of 2π at the wavelength λ.

In the visible region, a source such as a thermal source need only have a change in spectral width of approximately 2.5 μm in order to affect the temporal coherence reduction; in the submillimeter region, however, this number increases to fractions of a millimeter. Thus, the roughness of the surface must be considerably larger, or the spectral bandwidth requirements become much larger than are actually achievable.

A method for frequency-modulating the source is shown in Fig. 19. A submillimeter source is modulated by a phase modulator that has a high-frequency noise generator as a driver.

The effects of coherent imaging and incoherent imaging corresponding to temporal coherence reduction have been illustrated in the visible region (Ref. 13) and are indicated in Fig. 20. For white light, which has a large spectral bandwidth, and a small-f/number (i.e., a fast) system, the image is relatively clear; for white light and a large-f/number system, corresponding to the situation where the speckle size is increased, the image is degraded. Finally, Fig. 20 shows that for coherent light and a large-f/number system, the image quality is reduced considerably. In fact, the object is virtually impossible to recognize.

The effect of spectral integration in the visible region (Ref. 13) is illustrated in Fig. 21, which shows that the likelihood of recognition of the object is slightly enhanced when images made at two wavelengths are added. With the superposition of images made at four wavelengths, the improvement is evident. Finally, when 16 wavelengths are used, an easily recognizable image is obtained. Nevertheless, the resulting image is not as good as when a white light source is used.

B. SPATIAL COHERENCE REDUCTION

Two possible means of reducing the spatial coherence are (1) use of the natural effect of turbulence and (2) use of a diffuser at the receiver. Unfortunately, because the turbulence-induced random phase shift is a negligible quantity at submillimeter wavelengths, the coherence reduction using turbulence is not likely to be useful. The effect of using a diffuser in an imaging receiver has been studied (Ref. 13) and is shown in Fig. 22. This picture was obtained by moving a ground glass in the image plane and observing the temporally integrated effect. It is clear that the diffusing motion does improve the image, but

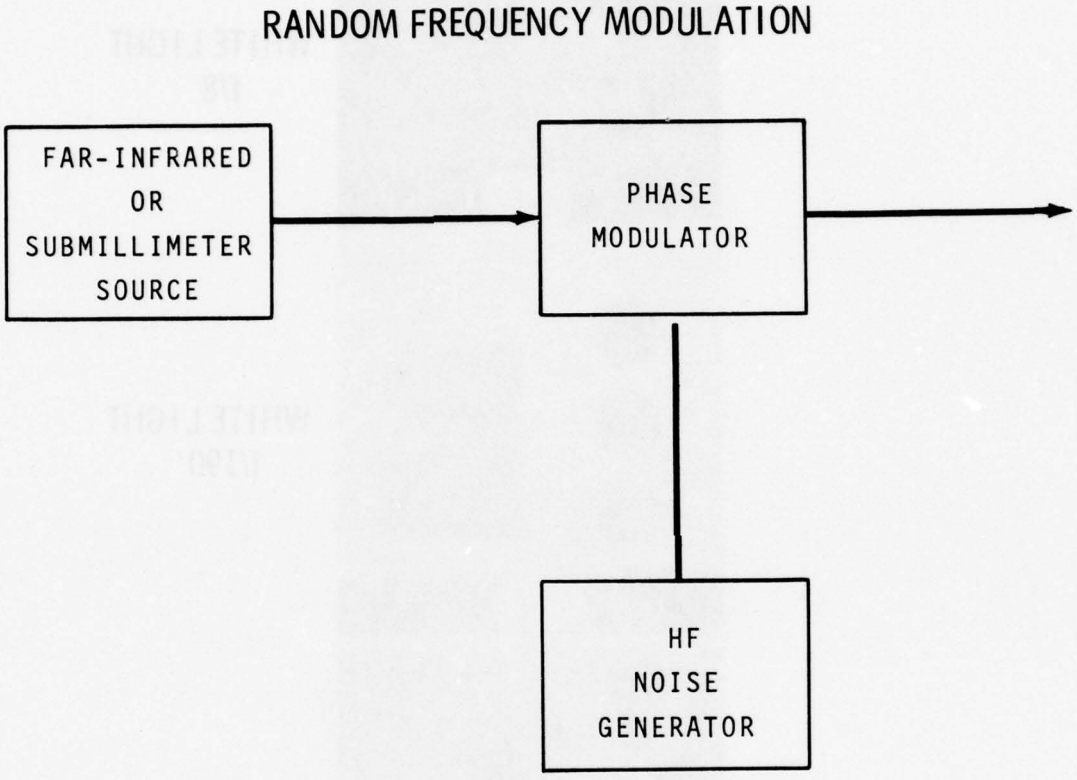

FIGURE 19. Block diagram of a possible technique for decreasing the temporal coherence of a highly coherent source.

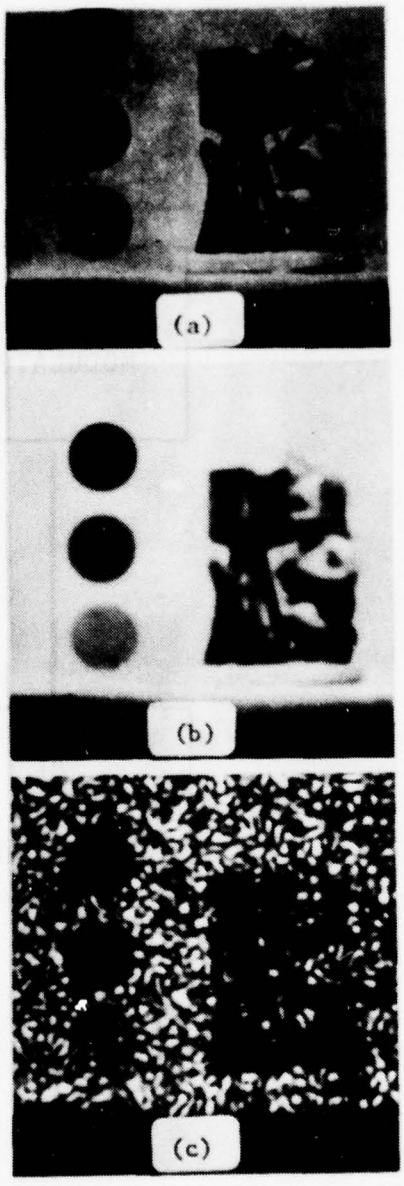

WHITE LIGHT
f/8

WHITE LIGHT
f/190

LASER
f/190

11-23-76-18

FIGURE 20. Photographs illustrating the difference between incoherent and coherent images. (Source: Ref. 13)

FIGURE 21. Photographs illustrating the smoothing effect on an image of spectral integration. (Source: Ref. 13)

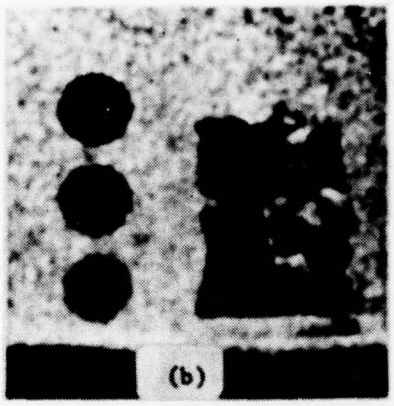

11-23-76-19

FIGURE 22. Photograph illustrating the smoothing effect on an image caused by effectively temporally averaging a time-varying speckle pattern. (Source: Ref. 13)

this concept may be somewhat impractical in the submillimeter region, especially in a situation where a line scanner is to be employed.

C. SPATIAL AVERAGING

One technique that can be considered to achieve spatial averaging in the far-infrared or the submillimeter region is the use of a large-aperture receiver with an observer. The effect of the large aperture can be seen in Fig. 23. Because of the large aperture relative to the focal length (small f/number), the speckle spot size is reduced in the visible region to the point where it is no longer discernible because of the lack of resolution of the eye. The observer therefore automatically spatially integrates the high spatial-frequency content of the scene. Whether an improvement can be achieved in the far-infrared or the submillimeter region to this extent is not clear, but some improvement by the use of a large aperture and spatial integration should be possible. Even if speckle reduction can be achieved by increasing the aperture, larger optics are not desirable if the signal level is sufficient for detection; i.e.,

11-23-76-20

FIGURE 23. Photograph showing decrease in speckle spot size due to a large-f/number system (aperture integration). (Source: Ref. 13)

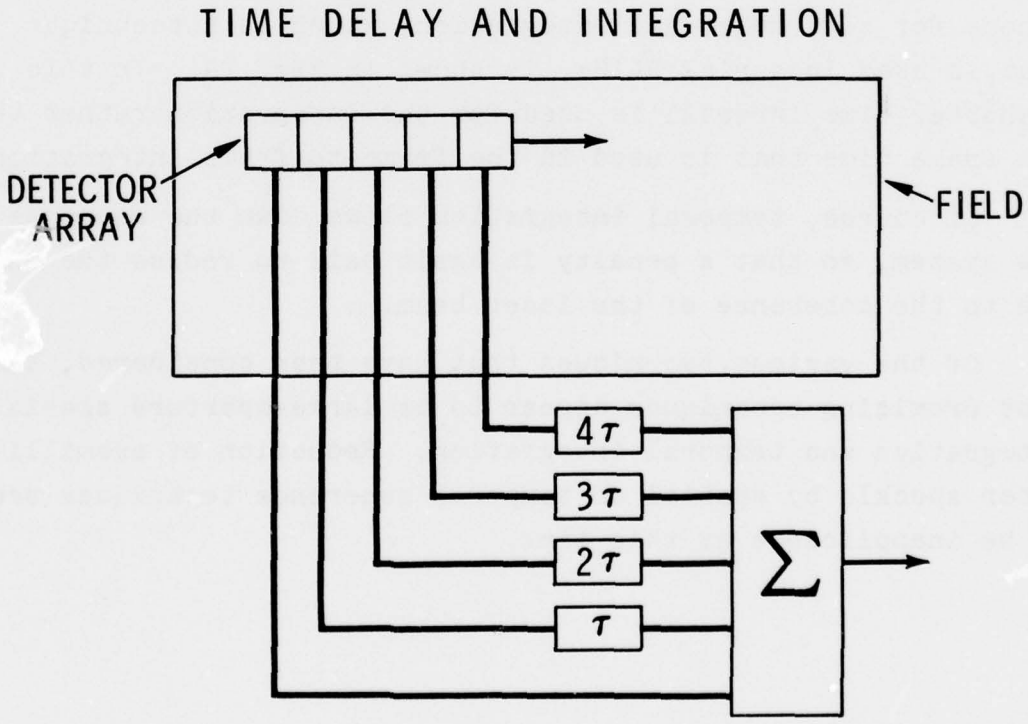

11-22-76-21

FIGURE 24. Block diagram of possible technique to average speckle patterns by time delay and integration.

increased optics to reduce speckle are an unwanted system burden that is not present in noncoherent systems. The rejection of high spatial frequencies by the eye to reduce the speckle results in an undersirable effect as well. It is that the resolution capability is decreased. When the system design is such that the eye is the system limitation, however, the design need not be improved.

D. TEMPORAL INTEGRATION

Two temporal integration techniques, frame-to-frame integration and time delay and integration, can be considered to reduce the speckle effect. In frame-to-frame integration, a superposition of one frame on another is used. The resulting reduction of the speckle effects is evident in Fig. 4. The scheme for time delay and integration, which is a technique that is used in serial FLIRs, is shown in Fig. 24. In this case, a shorter time interval is used for the integration rather than the frame time that is used in the frame-to-frame integration.

Of course, temporal integration slows down the response of the system, so that a penalty is again paid to reduce the noise due to the coherence of the laser beam.

Of the various techniques that have been considered, the most promising techniques appear to be large-aperture spatial integration and temporal integration. Reduction of submillimeter speckle by spatial or temporal coherence techniques seems to be inapplicable at this time.

IV. SPECULAR REDUCTION

The speckle effect has been shown to be amenable to some solution by a variety of techniques. The specular component, however, is somewhat more difficult to deal with. A possible way of decreasing the problem of the specular component is with electronic processing. For example, the technique of logarithmic amplification can be used to reduce the large peak values of the specular component relative to the scene information so that objects could be identified. In using logarithmic amplification, however, it should be recognized that the contrast between object and background is correspondingly reduced.

A potential advantage of logarithmic amplification is the fact that logarithmic processing essentially changes the multiplicative noise of the speckle to an additive noise. Consequently, it may be possible to filter the speckle component after logarithmic amplification of the spectra of the scene and the speckle terms are separated.

Another possibility would be to use an electronic limiting technique. In the limiting technique, only the large signals, corresponding to specular returns, would be suppressed and the contrast of the lower-level diffuse or speckle component relative to the background would not be affected.

A nonelectronic process for speckle reduction would be the use of polarization filtering. Although rough surfaces depolarize radiation, the specular component obeys Fresnel reflection laws so that the specular return should retain the polarization characteristics of the transmitted beam, which could be filtered with a polarizer.

V. SUMMARY AND CONCLUSION

This paper has addressed speckle and specular effects in long-wavelength active imaging systems. The analyses have produced the following results:

1. The general expression for coherent active imaging, including scene information, surface roughness, turbulence, and optics, has been derived.
2. A single expression for the speckle and specular components due to scattering from a rough surface has been obtained, and computer plots of the scattering diagrams, peak values, angular bandwidth, and relative integrated values have been determined. The equations and the plots determine the modification to the range equation that must be made to account for specular and speckle effects.
3. The correlation function for the speckle pattern has been obtained, and computer plots for various surfaces have been made.
4. The turbulence effect is expected to be negligible in the far-infrared and submillimeter regions for ranges less than 5 km because of the wavelength dependence.
5. The influence of optics has been considered, and the analysis indicates that a small-f/number system must be used in order to reduce the speckle effects.

6. Speckle reduction techniques have been considered, including the following generic techniques:

   - Decrease in spatial coherence
   - Decrease in temporal coherence
   - Aperture integration
   - Temporal integration.

   Of the various specific techniques considered, aperture integration and frame-to-frame or time delay and integration appear to be most promising.

7. Specular component reduction using nonlinear electronic processing techniques has been considered. These techniques essentially limit the peak values of the signal to suppress the specular component relative to other components.

In conclusion, the analysis has indicated that active imaging at long wavelengths is a difficult problem. That is not to say that it is impossible, but there are a number of problems that must be addressed before active imaging in the far-infrared and submillimeter regions can be considered to be a viable approach to the all-weather imaging requirements.

REFERENCES

1. Institute for Defense Analyses, *Laser-Aided FLIR Systems (LAFS) (U)*, IDA Paper P-1163, V. J. Corcoran, July 1976 (CONFIDENTIAL).

2. P. W. Kruse, *System for Imaging through Inclement Weather at Submillimeter Wavelengths*, paper presented at Conf. on Lasers and Electrooptical Systems, San Diego, California, May 25-27, 1976.

3. F. A. Rosell and R. H. Willson, "Recent Psychophysical Experiments and the Display Signal-to-Noise Ratio Concept," in L. M. Biberman, ed., *Perception of Displayed Information*, Plenum Press, New York, 1973.

4. J. D. Rigden and E. I. Gordon, "The Granularity of Scattered Optical Maser Light," *Proc. IRE*, Vol. *50*, 1962, p. 2367.

5. J. W. Goodman, "Statistical Properties of Laser Speckle Patterns," in J. C. Dainty, ed., *Laser Speckle and Related Phenomena*, Vol. *9* of *Topics in Applied Physics*, Springer-Verlag, Berlin Heidelberg, 1975, pp. 9-75.

6. See, for example, articles in special issue on speckle in optics, *J. Opt. Soc. Am.*, Vol. *66*, 1976, p. 1145.

7. T. S. McKechnie, "Speckle Reduction," in J. C. Dainty, ed., *Laser Speckle and Related Phenomena*, Vol. *9* of *Topics in Applied Physics*, Springer-Verlag, Berlin Heidelberg, 1975, pp. 123-170.

8. J. C. Dainty, ed., *Laser Speckle and Related Phenomena*, Vol. *9* of *Topics in Applied Physics*, Springer-Verlag, Berlin Heidelberg, 1975, p. 1.

9. M. J. Beran and G. B. Parrent, Jr., *Theory of Partial Coherence*, Prentice-Hall, Inc., Englewood Cliffs, N.J., 1964, p. 96.

10. P. Beckmann and A. Spizzichino, *The Scattering of Electromagnetic Waves from Rough Surfaces*, Pergamon Press, New York, 1963, pp. 182-184.

11. V. J. Corcoran and H. P. Ford, Jr., "Optical Heterodyne Detection of Radiation from Rough Surfaces," *IEEE Journal of Quantum Electronics*, June 1969, p. 292.

12. V. I. Tatarski, *Wave Propagation in a Turbulent Medium*, McGraw-Hill Book Company, Inc., New York, 1961, pp. 155-156.

13. N. George, "Speckle," *Optics News*, Vol. 2, No. 1, January 1976, pp. 14-20.

APPENDIX A

BACKGROUND ON SPECKLE

APPENDIX A

BACKGROUND ON SPECKLE

When the output radiation from the first gas lasers was observed after reflection from a wall, an unexpected graininess in the output was observed. The graininess or random intensity fluctuations observed in the image plane of an object illuminated by highly coherent light, as seen in Fig. A-1a, are called laser speckle. The Fresnel reflection ordinarily associated with the illumination of a smooth surface is a specular effect, which is illustrated in Fig. A-1b.

Laser speckle is due to the summation of radiation reflected from various portions of the illuminated object at points in the image plane. The introduction of path differences that are a significant fraction of a wavelength by scattering from various parts of the object results in intensity variations from image point to image point. The first gas laser operated at 1.15 μm, and an ordinary wall or a sheet of paper presents a rough surface for this wavelength at near-normal incidence. This is the reason these surfaces appear to be dull rather than shiny.

The first-order statistics of a speckle pattern have been obtained by assuming that the field at any point in the image plane containing the speckle pattern can be found by considering the field to be the sum of phasors whose amplitudes are statistically independent of each other and uniformly distributed in phase (Ref. A-3). The problem is considered to be statistically equivalent to a random-walk problem. Through the central limit theorem, the probability density function for the real and imaginary parts of the amplitude of the field is found to be

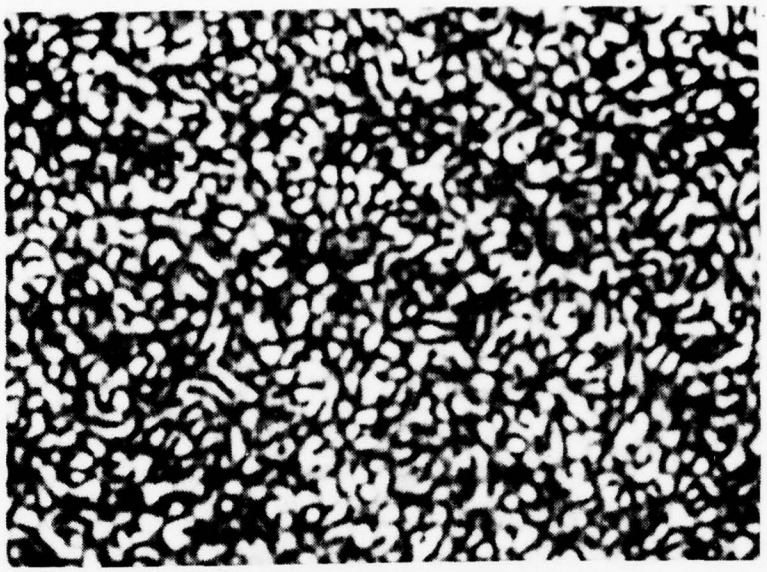

FIGURE A-1a. Laser speckle pattern.
(Source: Ref. A-1)

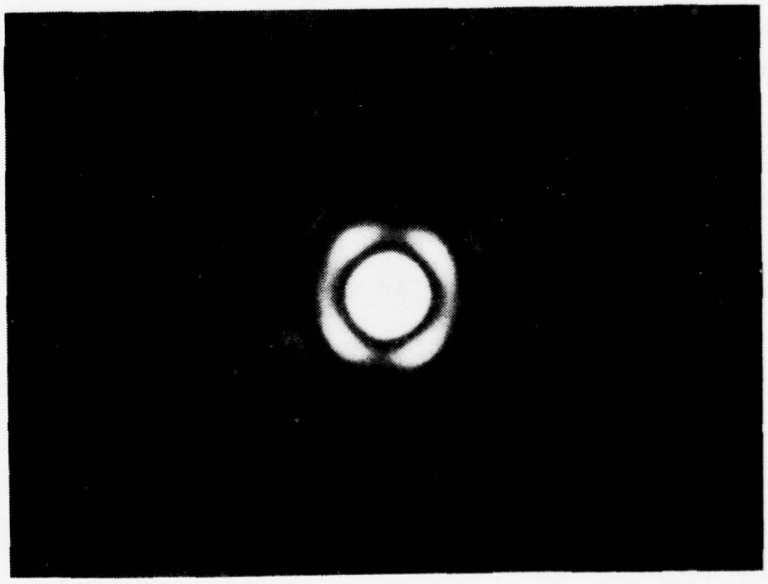

FIGURE A-1b. Airy disc pattern.
(Source: Ref. A-2)

$$p_{r,\,i}\left(A^{(r)},\, A^{(i)}\right) = \frac{1}{2\pi\sigma^2}\, e^{-\frac{A^{(r)2}+A^{(i)2}}{2\sigma^2}} \quad ,$$

where

$$\sigma^2 = \lim_{N\to\infty} \frac{1}{N} \sum_{k=1}^{N} \frac{\langle |a_k|^2 \rangle}{2} \quad .$$

From this expression the probability density function for the intensity becomes

$$P(I) = e^{-I/\langle I \rangle} \quad ,$$

which is plotted in Fig. A-2a. The probability density function for the phase is plotted in Fig. A-2b.

This expression does not take into account the effect that propagation has on the electric field, since the derivation is based on an assumed summation of fields in the image plane. Implicit in the assumptions that are made is that the illuminated surface is very rough.

The probability density function for the addition of two speckle patterns on an intensity basis is shown in Fig. A-3a. When the two patterns are perfectly correlated ($c_{12} = 1$), the statistics of the sum are the same as for a single pattern, since the patterns are identical. As the correlation decreases, the probability-density-function peak shifts to a higher intensity, i.e., a region of zero intensity is less likely to occur for the addition of two uncorrelated speckle patterns. The contrast, which is the ratio of the standard deviation to the average intensity, is a minimum at $\lambda_1 = 0.5$ for the sum of two speckle patterns as shown in Fig. A-3b. Addition of speckle patterns is of interest for averaging the effects of many patterns.

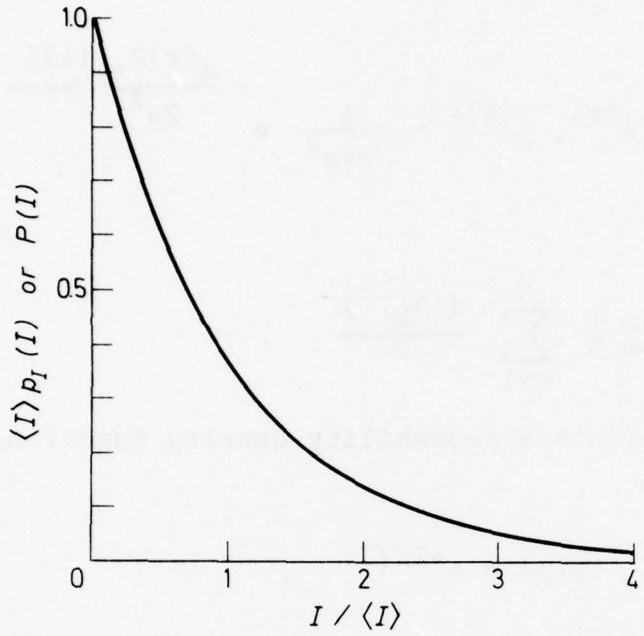

FIGURE A-2a. Normalized probability density function and probability that the intensity exceeds level I for a polarized speckle pattern. (Source: Ref. A-3)

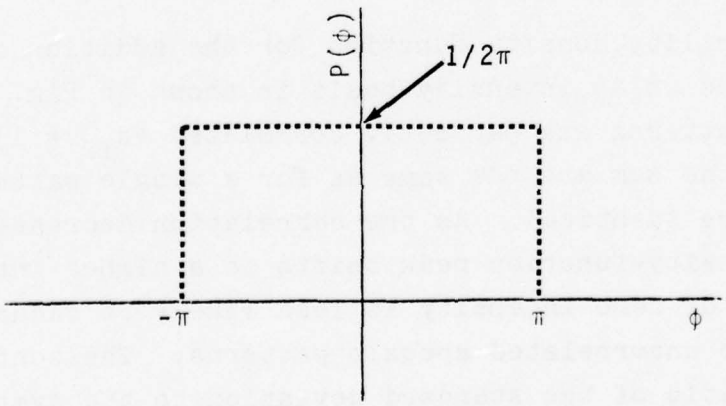

FIGURE A-2b. Normalized probability density function for the phase of a speckle pattern.

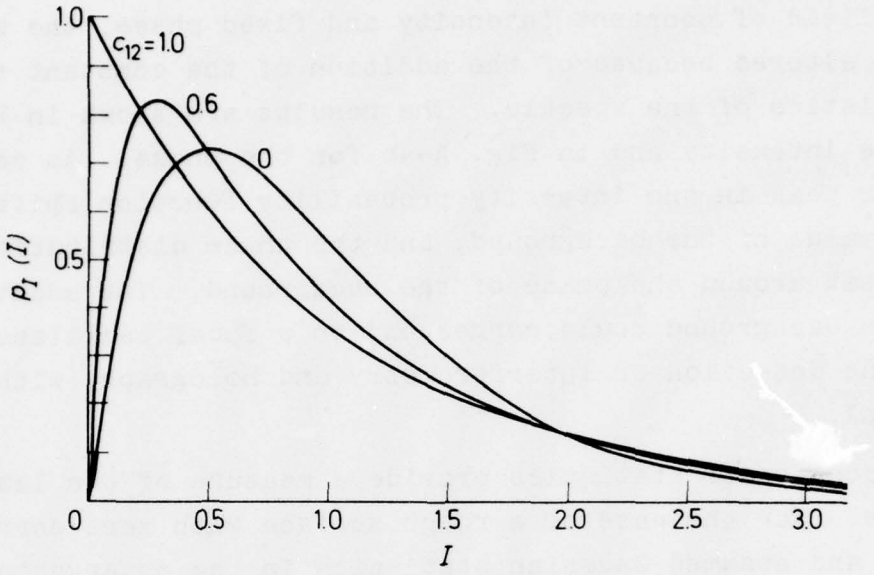

FIGURE A-3a. Probability density functions for intensity of the sum of two speckle patterns with $\langle I_1 \rangle = \langle I_2 \rangle = 1/2$ and $c_{12} = 0, 0.6, 1.0$, where c_{12} is the correlation function. (Source: Ref. A-3)

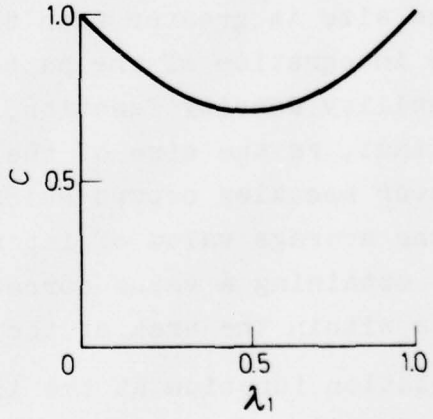

FIGURE A-3b. Contrast for sum of two speckle patterns with $\langle I \rangle = 1$, plotted as a function of λ_1, where λ_1 is the mean value of the second pattern, and $\lambda_1 + \lambda_2 = 1$ is the total mean intensity. (Source: Ref. A-3)

When the field of a speckle pattern is added to a uniform background field of constant intensity and fixed phase, the statistics are altered because of the addition of the constant term to the statistics of the speckle. The results are shown in Fig. A-4a for the intensity and in Fig. A-4b for the phase. As can be seen, the peak in the intensity probability function shifts toward the value of the background, and the phase distribution begins to peak around the phase of the background. The addition of a uniform background could correspond to a local oscillator in heterodyne detection or interferometry and holography with a strong signal.

The second-order statistics provide a measure of the laser speckle size. For the case of a rough surface with zero correlation length and assumed Gaussian statistics in the observation plane, the results for the correlation function are the same as obtained for a uniformly illuminated aperture. The statistics for the intensity and phase are shown in Fig. A-5. The similarity of the conditional probability to the probability functions for a speckle pattern added to a uniform background is evident.

When a detector whose size is greater than the average speckle size is used, the integration of the pattern by the detector results in a probability density function, as shown in Fig. A-6. It is evident that, as the size of the detector increases, an integration over speckles occurs which decreases the likelihood of obtaining the average value of intensity and increases the likelihood of obtaining a value corresponding to the average number of speckles within the area of the detector.

For an assumed correlation function at the illuminated surface, the field in the observation plane can be obtained in terms of the statistics of the surface roughness. For a Gaussian surface with a correlation function given in Fig. A-7a, the coherence factor at the surface depends on the surface fluctuations as shown in Fig. A-7b. The decrease in coherence area as the surface roughness increases for a fixed correlation length is evident, as has

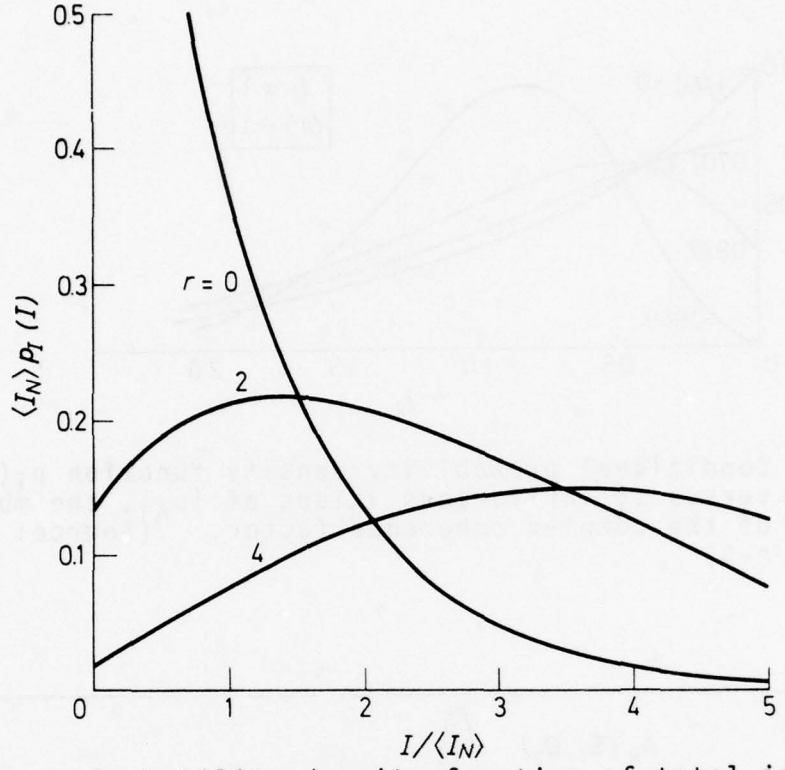

FIGURE A-4a. Probability density function of total intensity for a sum of a speckle pattern and a coherent background where r is the ratio of the background to the speckle, i.e., $r = I_S/\langle I_N \rangle$. (Source: Ref. A-3)

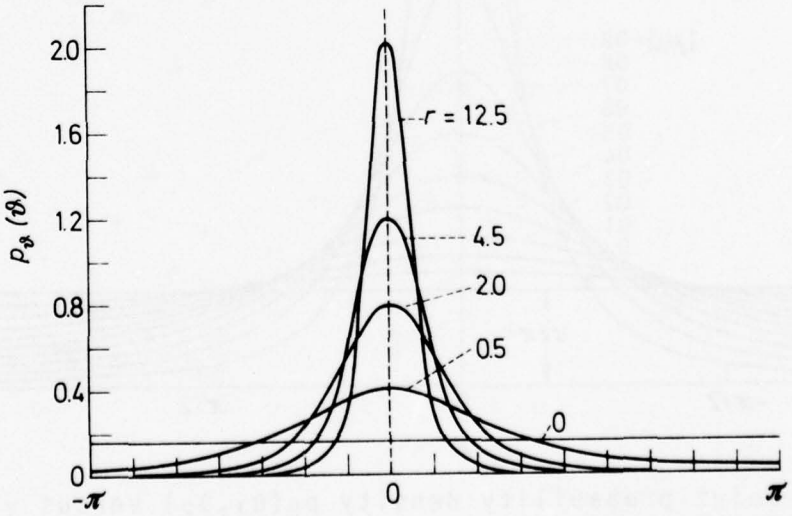

FIGURE A-4b. $p_\theta(\theta)$ versus θ for several values of the parameter $r = I_S/\langle I_N \rangle$. (Source: Ref. A-3)

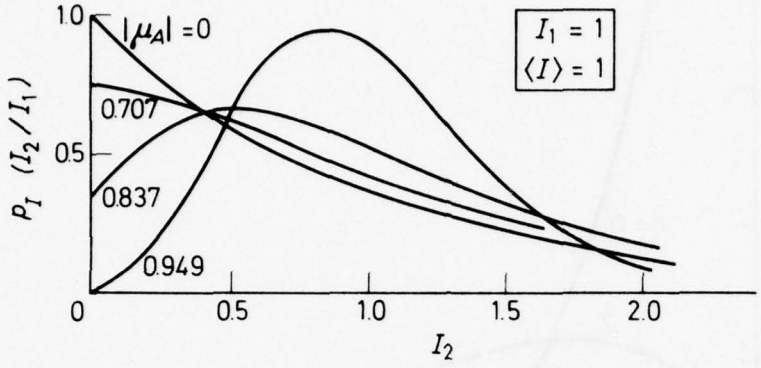

FIGURE A-5a. Conditional probability density function $p_I(I_2/I_1)$ versus I_2 for various values of $|\mu_A|$, the modulus of the complex coherence factor. (Source: Ref. A-3)

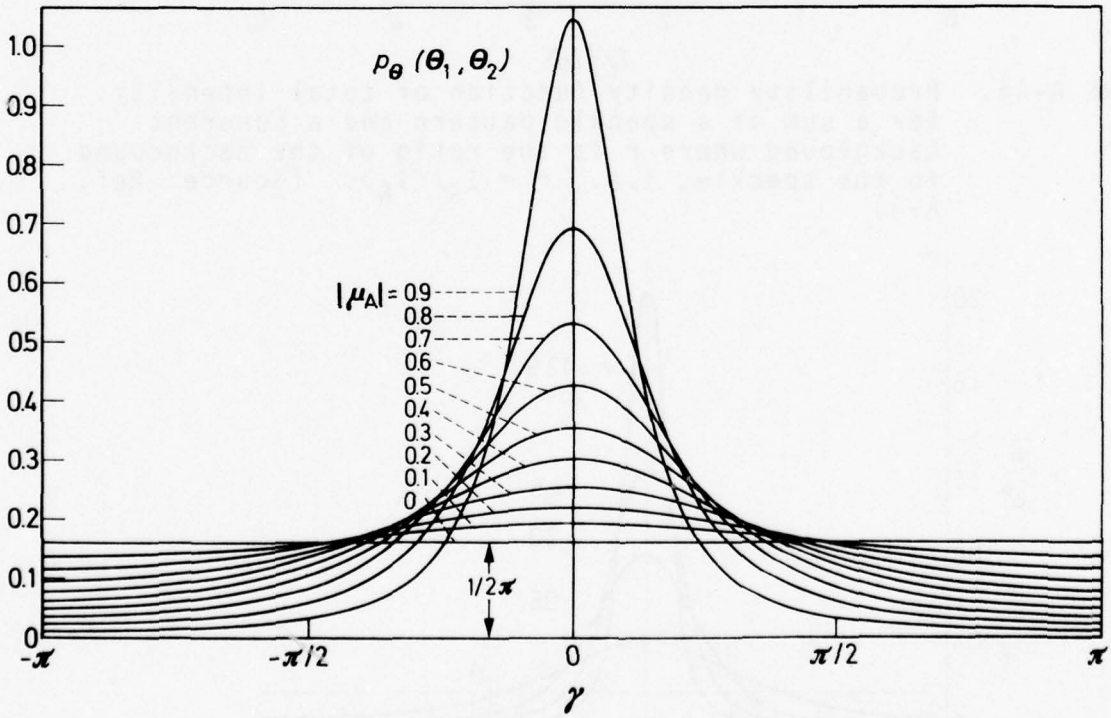

FIGURE A-5b. Joint probability density $p_\theta(\theta_1,\theta_2)$ versus $\gamma = \theta_2 - \theta_1 + \psi$ for various values of $|\mu_A|$. (Source: Ref. A-3)

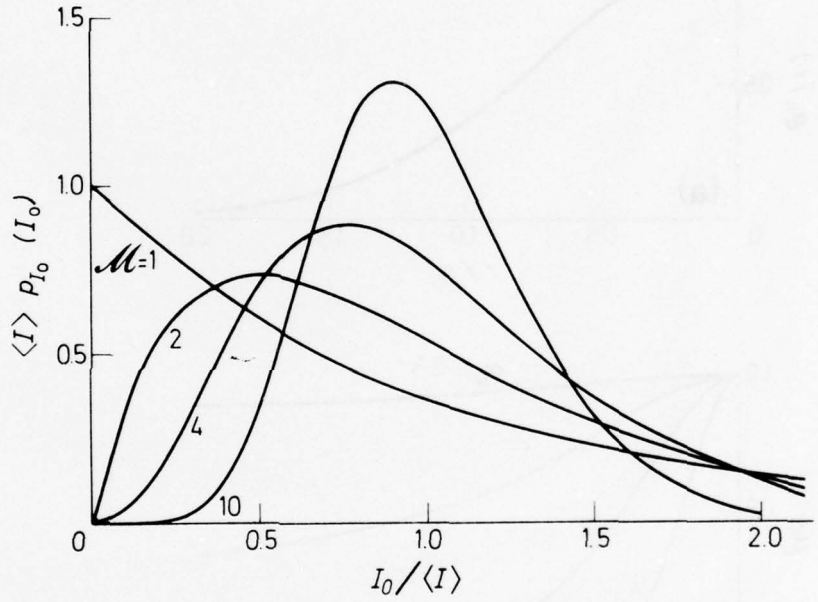

FIGURE A-6. Probability density function $p_{I_0}(I_0)$ for several values of the parameter M, the number of speckle correlation cells within the measurement aperture. (Source: Ref. A-3)

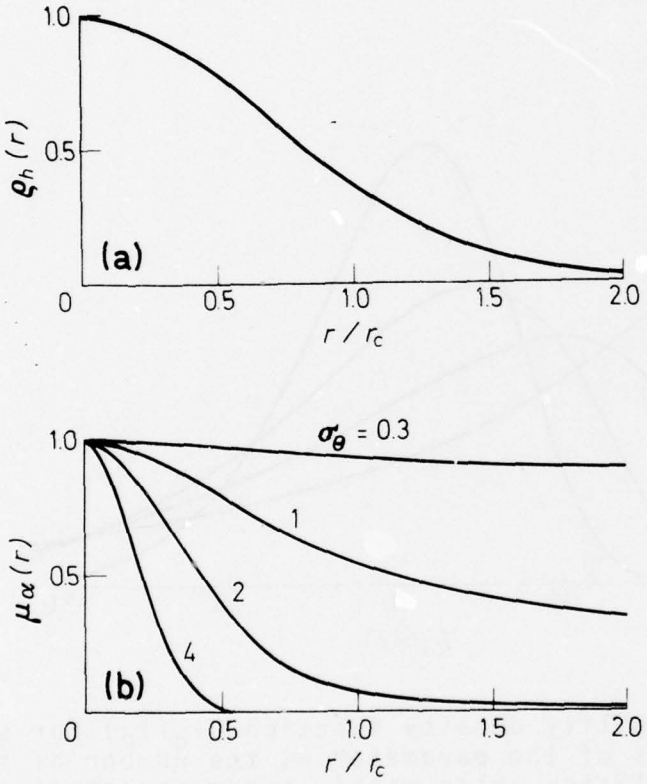

FIGURE A-7. Plots of (a) the assumed correlation function of the surface and (b) the corresponding complex coherence factor of the fields at the surface for several values of σ_θ^2, the variance of the phase angle which is related to the variance of the surface, i.e., the roughness. (Source: Ref. A-3)

previously been shown. As has been mentioned, the contrast is defined as

$$C = \sigma_I / \langle I \rangle \quad .$$

This value is plotted in Fig. A-8 for a Gaussian surface and various values of N, the number of correlation areas of the surface that contribute to the observed intensity.

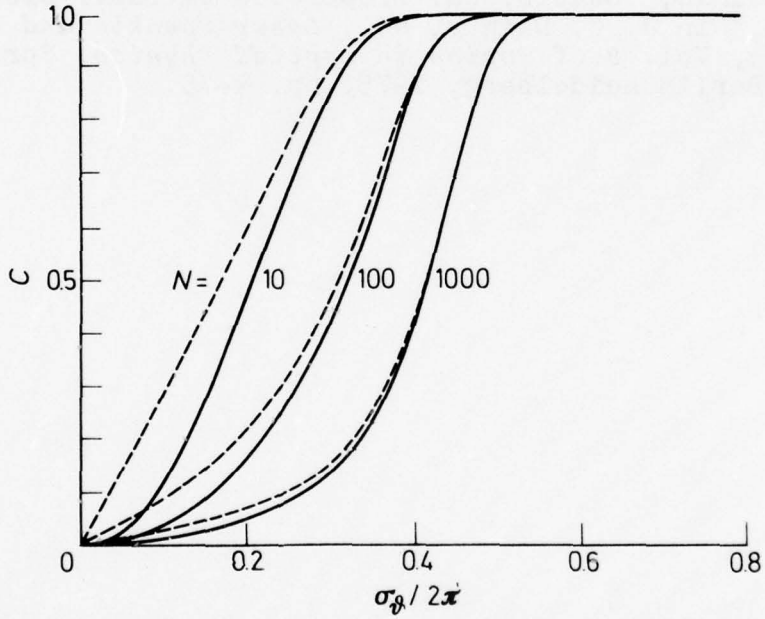

FIGURE A-8. Speckle contrast as a function of rms phase deviation, Gaussian surface correlation function assumed for various values of N, the number of correlation areas of the surface that contribute to the observed intensity. (Source: Ref. A-3)

REFERENCES, APPENDIX A

A-1. J. C. Dainty, ed., *Laser Speckle and Related Phenomena*, Vol. 9 of *Topics in Applied Physics*, Springer-Verlag, Berlin Heidelberg, 1975, p. 1.

A-2. M. J. Beran and G. B. Parrent, Jr., *Theory of Partial Coherence*, Prentice-Hall, Inc., Englewood Cliffs, N. J., 1964, p. 96.

A-3. J. W. Goodman, "Statistical Properties of Laser Speckle Patterns," in J. C. Dainty, ed., *Laser Speckle and Related Phenomena*, Vol. 9 of *Topics in Applied Physics*, Springer-Verlag, Berlin Heidelberg, 1975, pp. 9-75.

APPENDIX B

SPECKLE AND SPECULAR ANALYSIS

APPENDIX B

SPECKLE AND SPECULAR ANALYSIS

A. FIRST-ORDER STATISTICS

1. Current and Field Expressions

Infrared and submillimeter imaging systems, both those that are deployed and those that are proposed, transform radiation in the image plane of the receiver to electrical current by means of photon detectors. An imaging system may employ a single element as in a line scanner, a scanning array as in a FLIR, or a staring array as in focal-plane arrays under development. In each of these systems the scene information is transformed into current at the detector output. Current is therefore of interest in the analysis of an infrared imaging system.

The output current of an infrared or submillimeter detector can be expressed as (Ref. B-1):

$$i(t) = \frac{1}{T}\int_{t-T}^{t}\int_{A} R\left[V^{(r)}(P, t')\right]^2 dA\, dt' \qquad \text{(B-1)}$$

$$= \frac{1}{T}\int_{t-T}^{t}\int_{A} RV(P,t')\, V^{*}(P,t')\, dA\, dt'$$

$$+ \frac{1}{T}\int_{t-T}^{t}\int_{A} R(V^2 + V^{*2})\, dA\, dt' \quad ,$$

where R is the spatial responsivity of the detector and V(P,t') is the field at some point P and time t'. When the field at the detector surface is a single monochromatic wave, one has

$$V(P,t) = E(P)\, e^{-i\omega t} \quad , \tag{B-2}$$

where E represents the spatial variation of the field, and the integration time of the detector is such that $1/T < \omega$, i.e., the integration time is larger than the period of the electromagnetic wave, and the detector output current is

$$i(t) = \int_A R\, E(P)E^*(P)\, dA \quad . \tag{B-3}$$

When the output current is statistical in nature, the ensemble average of the current is of interest. It is given by

$$\langle i(t) \rangle = \int_A R\, \langle E(P)E^*(P) \rangle\, dA \quad . \tag{B-4}$$

Equation B-4 represents the statistical average of the current that would be obtained by measuring the current with the detector centered at P for each member of the ensemble.

With a knowledge of the spatial variation of the electric field and the detector responsivity across the detector surface, the output current for the problem of interest can be calculated from Eq. B-4. The detector output current can be found, therefore, by determining the average power in the detector plane and integrating over the detector surface.

The electric field in the detector plane for the case where a surface has been illuminated by monochromatic radiation is determined by summing at each point in the plane in front of the optics the radiation propagated from each point on the scattering surface and then determining the effect of the optics on the field.

The analysis here is limited to a two-dimensional surface. The extension to a three-dimensional surface is obvious for a rectangular or cylindrical coordinate system, and the analysis of the three-dimensional surface merely complicates the equations without substantially changing the results. A two-dimensional scattering surface can be depicted as in Fig. B-1, where radiation from the direction θ_1 illuminates a surface whose contour is given by $\zeta(\xi)$ and the field in the direction θ_2 is desired.

When the Fresnel-Kirchhoff diffraction integral is used to express the effect of propagation on the electric field, the field at a point y in the lens plane is given by (Ref. B-2)

$$E(y) = \frac{1}{i\lambda} \frac{\cos \delta}{r} \int_{\xi} A(\xi)\, e^{ikr}\, d\xi \quad , \tag{B-5}$$

where $A(\xi)$ describes the scene information
$\cos \delta$ is the obliquity factor
k is the wave vector factor
r is the distance from point ξ to point y.

That it is a reasonable approximation to take the obliquity factor outside the integral can be seen by considering the value of cos δ for any infrared imaging system with a laser illuminator. Even for a 100-mr system, cos δ is close to 1 at the extremities. Now, r is given by

$$r^2 = (z + \Delta z)^2 + [y - (\xi + y_1)]^2 \quad , \tag{B-6}$$

which can be expanded in a series whose first two terms yield

$$r = r_o + \Delta z \cos \theta_2 + \xi \sin \theta_2 - y \sin \theta_2 + \frac{\xi^2 + y^2 - 2\xi y}{2r_o} \quad , \tag{B-7}$$

where

$$r_o = z^2 + y_1^2 \quad .$$

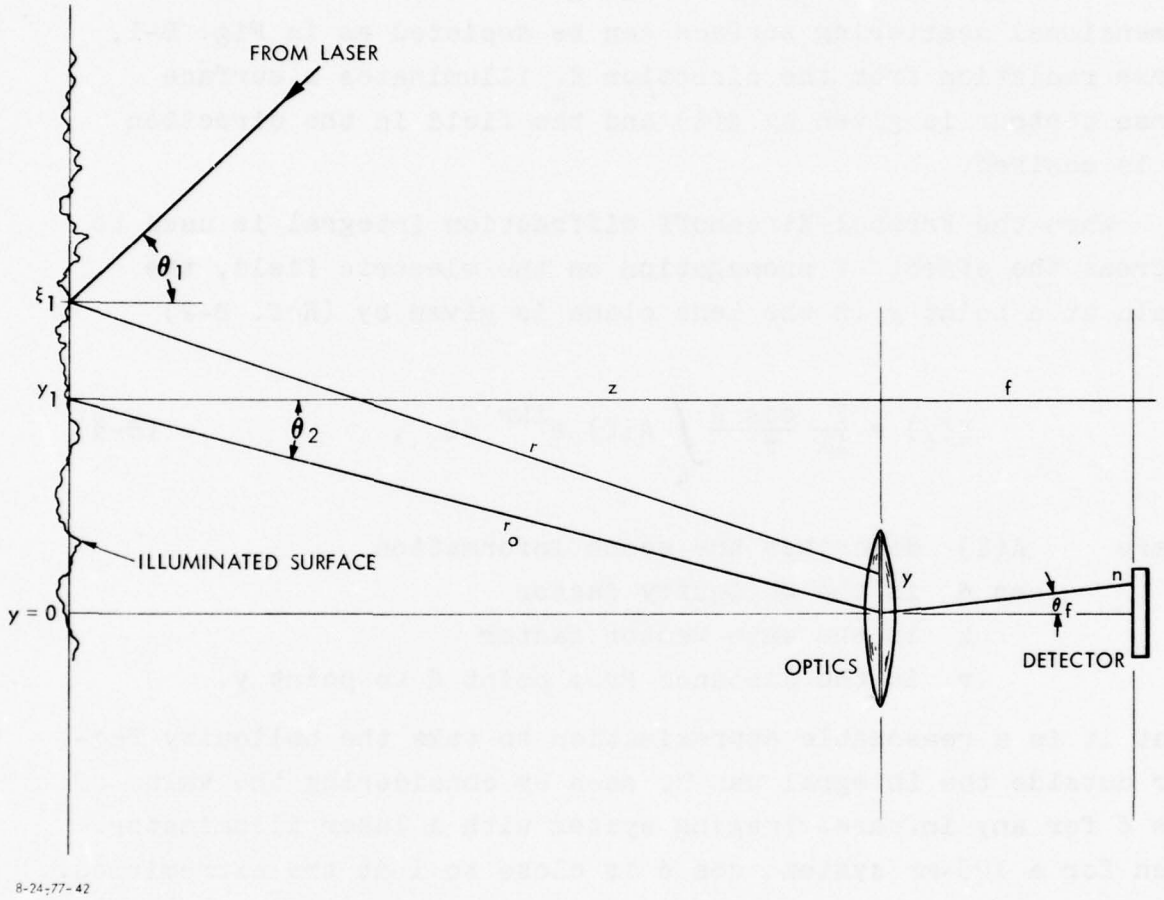

FIGURE B-1. Geometry for analysis of detection of laser radiation scattered from a rough surface.

The wave number k is given by

$$k = 2\pi (n_o + \Delta n) f/c = k_o + \Delta k \qquad \text{(B-8)}$$

to account for variations in the index of refraction of the medium. The electric field at y is then

$$E(y) = \frac{1}{i\lambda r}\int A(\xi)\, e^{i(k_o+\Delta k)(r_o+\Delta z\cos\theta_2 + \xi\sin\theta_2 - y\sin\theta_2 + \frac{\xi^2+y^2-2y\xi}{2r_o})} e^{i\phi}\, d\xi$$

$$= \frac{1}{i\lambda r}\int A(\xi)\, e^{ik_o(r_o+\Delta z\cos\theta_2+\xi\sin\theta_2-y\sin\theta_2+\frac{\xi^2+y^2-2y\xi}{2r_o})} e^{i\Delta k r_o}\, e^{i\phi}\, d\xi\,, \qquad \text{(B-9)}$$

where ϕ accounts for the phase shift of the radiation upon reflection, and the obliquity factor is assumed to be 1. This has been shown to be a good approximation for active infrared imaging systems.

2. Mean Square Field Expression

The mean square of the field at a point y in the Fresnel region is

$$\langle E(y)E^*(y)\rangle = \int_{\xi_2}\int_{\xi_1} A(\xi_1)A(\xi_2^*)\, \langle e^{ik_o\left[\Delta z(\xi_1)\cos\theta_2 - \Delta z(\xi_2)\cos\theta_2\right]} e^{i\left[\phi(\xi_1)-\phi(\xi_2)\right]}\rangle$$

$$\cdot \langle e^{ik_o\left[\Delta k(\xi_1)-\Delta k(\xi_2)\right]}\rangle\, e^{ik_o\frac{(\xi_1^2-\xi_2^2)}{2r_o}}$$

$$e^{ik_o\sin\theta_2(\xi_1-\xi_2)} e^{-ik_o 2\frac{(y\xi_1-y\xi_2)}{2r_o}}\, d\xi_1 d\xi_2$$

$$= \int_{\xi_2}\int_{\xi_1} A(\xi_1)A^*(\xi_2)\, R(\xi_1,\xi_2)\, T(\xi_1,\xi_2)\, e^{ik_o\frac{(\xi_1^2-\xi_2^2)}{2r_o}}$$

$$\cdot e^{ik_o\sin\theta_2(\xi_1-\xi_2)}\, e^{-ik_o\frac{2y(\xi_1-\xi_2)}{2r_o}}\, d\xi_1 d\xi_2\,, \qquad \text{(B-10a)}$$

where

$$R(\xi_1,\xi_2) = \langle e^{ik_o[\Delta z(\xi_1)\cos\theta_2 - \Delta z(\xi_2)\cos\theta_2}\, e^{i[\phi(\xi_1)-\phi(\xi_2)]}\rangle$$

is the term due to roughness and

$$T(\xi_1,\xi_2) = \langle e^{ik_o[\Delta k(\xi_1) - \Delta k(\xi_2)]}\rangle \text{ is the turbulence term.}$$

In the Fraunhofer region or far field, this expression reduces to

$$\langle E(y)E^*(y)\rangle = \int_{\xi_2}\int_{\xi_1} A(\xi_1)A^*(\xi_2)\, R(\xi_1,\xi_2)\, T(\xi_1,\xi_2)\, e^{ik_o \sin\theta_2(\xi_1-\xi_2)}\, d\xi_1 d\xi_2, \tag{B-10b}$$

which is a considerably simpler expression because of the elimination of the quadratic terms. In Eq. B-10 the term $1/(\lambda r)^2$ has been dropped for convenience, since it is the normalized value that is of interest.

A lens acts as a phase shifter for an incident wave, so that the field on one side of the lens is related to the field on the other side, as depicted in Fig. B-2, by (Ref. B-3)

$$E_o(y) = t(y)P(y)E_i(y) \quad ,$$

where

$$t(y) = e^{ikn\Delta_o}\, e^{-i\frac{k}{2f}y^2}$$

and

$$P(y) = 1 \quad |y| < D/2 \quad .$$

To determine the field in the focal plane of the lens, the Fresnel approximation to the Fresnel-Kirchhoff integral is used, so that

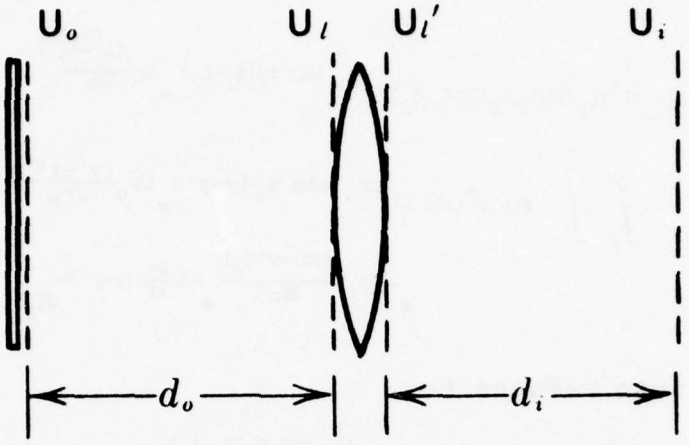

FIGURE B-2. Geometry for image formation. [Source: *Introduction to Fourier Optics* by J.W. Goodman (Ref. B-4). Copyright (c) 1968 by McGraw-Hill Book Company. Used with permission of McGraw-Hill Book Company.]

$$E_f(\eta) = \frac{e^{i\frac{k}{2f}\eta^2}}{i\lambda f}\int E_o(y)\, e^{i\frac{k}{2f}y^2}\, e^{-i\frac{2\pi}{\lambda f}y\eta}\, dy$$

$$= \frac{e^{i\frac{k}{2f}\eta^2}}{i\lambda f}\int E_1(y)\, P(y)\, e^{-i\frac{2\pi}{\lambda f}y\eta}\, dy \quad , \qquad \text{(B-11a)}$$

where the constant phase delay Δ_o is ignored.

When the value of the field from Eq. B-9 is substituted into Eq. B-11a, one obtains

$$E(\eta) = \frac{e^{i\frac{k\eta^2}{2f}}}{i\lambda f}\int_y P(y)\left[\int A(\xi) e^{ik_o\left(r_o+\Delta z\cos\theta_2+\xi\sin\theta_2-y\sin\theta_2+\frac{\xi^2+y^2-2y\xi}{2r_o}\right)} e^{i\Delta k r_o}\, e^{i\Phi}\, d\xi\right] e^{-i\frac{2\pi}{\lambda f}y\eta}\, dy \qquad \text{(B-11b)}$$

and the mean square field in the Fresnel region is then

$$\langle E(\eta)E^*(\eta)\rangle = \int_{\xi_2}\int_{\xi_1} A(\xi_1)A^*(\xi_2)R(\xi_1,\xi_2)T(\xi_1,\xi_2)\, e^{ik_o \sin\theta_2(\xi_1-\xi_2)}\, e^{ik_o\frac{(\xi_1^2-\xi_2^2)}{2r_o}}$$

$$\cdot \int_{y'}\int_{y} P(y)P^*(y')\, e^{-ik_o \sin\theta_2(y-y')}\, e^{ik_o\frac{(y^2-y'^2)}{2r_o}}$$

$$e^{-2ik_o\frac{(y\xi_1-y'\xi_2)}{2r_o}}\, e^{-i\frac{2\pi}{\lambda f}(y-y')\eta}\, d\xi_1 d\xi_2 dy\, dy' \quad . \text{(B-12a)}$$

In the far field this reduces to

$$\langle E(\eta)E^*(\eta)\rangle = \int_{\xi_2}\int_{\xi_1} A(\xi_1)A^*(\xi_2)R(\xi_1,\xi_2)T(\xi_1,\xi_2)\, e^{ik_o \sin\theta_2(\xi_1-\xi_2)}\, d\xi_1 d\xi_2$$

$$\cdot \int_{y'}\int_{y} P(y)P^*(y')\, e^{-ik_o(\sin\theta_2+\sin\theta_f)(y-y')}\, dy dy' \quad . \qquad \text{(B-12b)}$$

Notice that in the far field the integration over the scene is independent of the integration over the pupil function if the quadratic terms are ignored, while in the Fresnel region these integrals are coupled by the term

$$e^{-2ik_o\frac{(y\xi_1-y'\xi_2)}{2r_o}} \quad .$$

The independence of the integrals in the far field is due to the fact that in the far field the phase variations caused by the coupling term are negligible, or from another viewpoint the radiation in the y plane effectively comes from a point at ∞, so the phase variations depend only on θ_2. In either case, the mean square field in the focal plane, and therefore the mean current detector output, depends on the product of the scene information, the roughness, and the turbulence, i.e., upon

$$A(\xi_1)A^*(\xi_2)R(\xi_1,\xi_2)T(\xi_1,\xi_2) \quad .$$

Equations B-12a and B-12b can be considered to be the general two-dimensional expressions to be inserted into Eq. B-4 to determine the output current of a detector in an imaging system using one or more detectors. Equations B-12a and B-12b can easily be extended to three dimensions by including the other geometrical dimension in Eq. B-6 before proceeding. Equation B-12 can be recognized as the product of two equations that are in the form of Fourier transforms. The average output current from the detector can, therefore, be considered as a convolution of a term that describes the scene, a term that describes the surface roughness, and a term that describes the turbulence effects. This convolution is multiplied by a function describing the effect of the receiver. From this equation, it is evident that the speckle can be considered to be a multiplicative noise effect because of the fact that the roughness term is convolved with the scene term.

3. Roughness Considerations

If, for the time being, the scene information and the turbulence effects are ignored, the effect of only the roughness on the field in the focal plane can be determined from Eq. B-12b by the expression

$$\langle E(y)E^*(y)\rangle = \int_{\xi_2}\int_{\xi_1} R(\xi_1,\xi_2)\, e^{ik_o \sin\theta_2(\xi_1-\xi_2)}\, d\xi_1 d\xi_2$$

$$= \int_{\xi_2}\int_{\xi_1} \langle e^{ik_o[\Delta z(\xi_1)\cos\theta_2 - \Delta z(\xi_2)\cos\theta_2]} e^{i[\phi(\xi_1)-\phi(\xi_2)]}\rangle$$

$$e^{ik_o \sin\theta_2(\xi_1-\xi_2)}\, d\xi_1 d\xi_2 \ .$$

This expression can be written as

$$\langle E(y)E^*(y)\rangle = \int_{\xi_2}\int_{\xi_1} \langle e^{ik_o\cos\theta_2[\zeta(\xi_1)-\zeta(\xi_2)]}\rangle e^{ik_o \sin\theta_2(\xi_1-\xi_2)}\, d\xi_1 d\xi_2 \ , \qquad \text{(B-13)}$$

where the functions $\zeta(\xi_1)$ and $\zeta(\xi_2)$ account for the roughness of the scattering surface and include the phase-shift effects on the field upon reflection.

It is convenient to compare the field obtained in a given situation to what would be obtained at the Fresnel angle when the illuminating radiation is reflected by a smooth, perfectly conducting surface.

The normalized electric field at P is given by

$$\rho = \frac{F_2}{2L} \int_{-L}^{L} e^{ikr}\, d\xi \ , \qquad \text{(B-14)}$$

where L is the length of the linear surface

$$\rho = E/E_o$$

and

$$F_2 = \sec\theta_1 \frac{1 + \cos(\theta_1 + \theta_2)}{\cos\theta_1 + \cos\theta_2} \ .$$

The term $\langle e^{ik_o \cos\theta_2[\zeta(\xi_1) - \zeta(\xi_2)]} \rangle$ can be recognized as the characteristic function of the two-dimensional probability density function of the surface roughness, so that

$$\langle \rho(y)\, \rho^*(y) \rangle = \frac{F_2 F_2^*}{4L^2} \int_{-L}^{L} \int \chi_2(k_z, -k_z)\, e^{ik_x(\xi_1 - \xi_2)}\, d\xi_1 d\xi_2 \ . \qquad \text{(B-15)}$$

Equation B-15 is the general solution to be inserted into Eq. B-4. It should be noted that the mean square field has been related to the characteristic function of the surface. Eq. B-15 has previously been analyzed by deriving $\chi_2 (k_z, -k_z)$ for a Gaussian surface (Ref. B-5). The expression can be obtained as a special case of the expression $\chi_2 (k_{z1}, -k_{z2})$, which is now derived. This is done not merely as an exercise, but because the more general expression is needed for the second-order statistics.

4. Surface With Gaussian Statistics

One random process for which the two-dimensional characteristics function can be found analytically is the normally distributed random process. The probability density function for a normally distributed surface is given by

$$w(z) = \frac{1}{\sigma\sqrt{2\pi}} e^{-z^2/2\sigma^2} ,$$

and the characteristic function is

$$\chi(k_z) = e^{-\sigma^2 k_z^2/2} .$$

The joint probability density function for a normal distribution is given by

$$W(z_1,z_2) = \frac{1}{2\pi\sigma^2\sqrt{1-C}} \exp \frac{-z_1^2+2Cz_1z_2-z_2^2}{2\sigma^2(1-C^2)} , \qquad \text{(B-16)}$$

where σ is the standard deviation, the mean is zero, and the random variables are related by the correlation coefficient C. The characteristic function is

$$\chi_2(k_{z1}, -k_{z2}) = \int_{-\infty}^{\infty}\int_{-\infty}^{\infty} W(z_1,z_2)\, e^{k_{z1}z_1}\, e^{-ik_{z2}z_2}\, dz_1 dz_2$$

$$= \frac{1}{2\pi\sigma^2\sqrt{1-C^2}} \int_{-\infty}^{\infty}\int_{-\infty}^{\infty} e^{\frac{-z_1^2+2Cz_1z_2-z_2^2}{2\sigma^2(1-C^2)}}\, e^{ik_{z1}z_1}\, e^{ik_{z2}z_2}\, dz_1 dz_2$$

$$= e^{-\frac{\sigma^2}{2}(k_{z1}^2-2Ck_{z1}k_{z2}+k_{x2}^2)} \quad . \tag{B-17}$$

For the special case where $k_{z1} = k_{z2}$, one obtains

$$\chi_2(k_z,-k_z) = e^{-k_z^2\sigma^2(1-C)} \quad . \tag{B-18}$$

If it is assumed the autocorrelation coefficient is of the form $e^{-\tau^2/T^2}$, where T is the correlation length, then the characteristic function can be written as

$$\chi_2(k_{z1},-k_{z2}) = e^{-\frac{\sigma^2}{2}(k_{z1}^2+k_{z2}^2)}\, e^{\sigma^2 k_{z1}k_{z2}e^{-\tau^2/T^2}}$$

$$= e^{-\frac{\sigma^2}{2}(k_{z1}^2+k_{z2}^2)} \sum_{m=0}^{\infty} \frac{[\sigma^2 k_{z1}k_{z2}\, e^{-\tau^2/T^2}]^m}{m!}$$

$$= e^{-\frac{\sigma^2}{2}(k_{z1}^2+k_{z2}^2)} \sum_{m=0}^{\infty} \frac{\sigma^{2m} k_{z1}^m k_{z2}^m e^{-m\tau^2/T^2}}{m!} \quad , \tag{B-19}$$

which for $k_{z1} = k_{z2}$ is

$$\chi_2(k_z,-k_z) = e^{-\sigma^2 k_z^2} \sum_{m=0}^{\infty} \sigma^{2m} k_z^{2m}\, e^{-m\tau^2/T^2} \quad . \tag{B-20}$$

Finally, if $\tau = \xi_1 - \xi_2$,

$$\chi_2(k_{z1}, -k_{z2}) = e^{-\frac{\sigma^2}{2}(k_{z1}^2 + k_{z2}^2)} \cdot \sum_{m=0}^{\infty} \frac{\sigma^{2m} k_{z1}^m k_{z2}^m}{m!} \exp\left[\frac{-m}{T^2}\xi_1^2 + \frac{2m}{T^2}\xi_1\xi_2 - \frac{m}{T^2}\xi_2^2\right] \quad \text{(B-21)}$$

$$\chi_2(k_z, -k_z) = e^{-\sigma^2 k_z^2} \sum_{m=0}^{\infty} \frac{\sigma^{2m} k_z^{2m}}{m!} e^{\left[\frac{-m}{T^2}\xi_1^2 + \frac{2m}{T^2}\xi_1\xi_2 - \frac{m\xi_2^2}{T^2}\right]} \quad . \quad \text{(B-22)}$$

By substitution of Eq. B-22 into Eq. B-15, the ensemble average for a normally distributed surface can be determined. The equation then becomes

$$\langle \rho(y)\rho^*(y) \rangle = K \int_{-L}^{L} e^{\frac{-m}{T^2}\xi_2^2} e^{-ik_x\xi_2} \int_{-L}^{L} e^{\frac{-m}{T^2}\xi_1^2} e^{i\left(k_x - \frac{2mi}{T^2}\xi_2\right)\xi_1} d\xi_1 \, d\xi_2 \quad ,$$

where

$$K = \frac{F_2' F_2^*}{4L^2} e^{-\sigma k_z^2} \sum_{m=o}^{\infty} \frac{\sigma^{2m} k^{2m}_z}{m!} \quad .$$

This equation can be solved exactly by using an aperture function and extending the limits of integration to $\pm \infty$. A more expedient approach is to assume that $T << L$, i.e., that the correlation length is much less than the linear surface length, which will usually be true for the cases of interest, so that little error will result when the limits of integration are extended without the aperture function. With these conditions, one obtains

$$\langle \rho(y)\rho^*(y)\rangle = K\int_{-L}^{L} e^{\frac{-m}{T^2}\xi_2^2} e^{-ik_x\xi_2} \int_{-\infty}^{\infty} e^{\frac{-m}{T^2}k_1^2} e^{i(k_x\frac{-2mi}{T^2}\xi_2)\xi_1} d\xi_1 d\xi_2$$

$$= KT\sqrt{\frac{\pi}{m}}\int_{-L}^{L} e^{\frac{-m}{T^2}\xi_2^2} e^{-ik_x\xi_2} e^{-\frac{T^2}{4m}(k_x - i\frac{2m}{T^2}\xi_2)^2} d\xi_2$$

$$= \frac{\sqrt{\pi}T}{2L} F_2F_2^* e^{-\sigma^2 k_z^2} \cdot \sum_{m=0}^{\infty} \frac{\sigma^{2m} k_z^{2m}}{\sqrt{m}\, m!} e^{-\frac{T^2 k_x^2}{4m}} . \qquad \text{(B-23)}$$

Note that from m = 0 this expression diverges. This problem can be eliminated by subtracting $\chi(\rho)\ \chi^*(\rho)$ at the beginning of the derivation and reinserting it after the operations have been performed.

Instead of $\langle \rho\rho^* \rangle$, the square of the mean must be subtracted. Then one has

$$D\langle \rho\rho^* \rangle = \langle \rho\rho^* \rangle - \langle \rho \rangle \langle \rho^* \rangle$$

$$= \frac{F_2F_2^*}{4L^2}\int_{-L}^{L}\int_{-L}^{L} e^{ik_x\xi_1} e^{-ik_x\xi_2}\left[\chi_2(k_z, -k_z) - \chi(k_z)\chi^*(k_z)\right] d\xi_1 d\xi_2 .$$

Now $[\chi_2(k_z - k_z) - \chi(k_z)\ \chi^*(k_z)]$ is given by

$$[\chi_2(k_z, -k_z) - \chi(k_z)\ \chi^*(k_z)] = e^{-g}\sum_{m=1}^{\infty} \frac{g^m}{m!} e^{-m\tau^2/T^2} ,$$

so that

$$D(\rho) = \frac{F^2}{2L}\int_{-\infty}^{\infty} e^{ik_x - g} \sum_{m=1}^{\infty} \frac{g^m}{m!} e^{-m\tau^2/T^2} d\tau$$

$$= \frac{\sqrt{\pi}\, F^2 T}{2L} e^{-g} \sum_{m=1}^{\infty} \frac{g^m}{m!\sqrt{m}} e^{-k_x^2 T^2/4m} \qquad \text{(B-24)}$$

The mean power then becomes (Ref. B-5)

$$\langle \rho\rho^* \rangle = D\{\rho\} + \langle \rho \rangle \langle \rho^* \rangle$$

$$\langle \rho\rho^* \rangle = F^2 e^{-g} \left(\rho\rho^2 + \frac{\sqrt{\pi}T}{2L} \sum_{m=1}^{\infty} \frac{g^m}{m!\sqrt{m}} e^{-k_x^2 T^2/4m} \right), \quad \text{(B-25)}$$

where

$$F = \sec \theta_1 \frac{1 + \cos(\theta_1 + \theta_2)}{\cos \theta_1 + \cos \theta_2}$$

$$g = \left[2\pi \frac{\sigma}{\lambda} (\cos \theta_1 + \cos \theta_2)\right]^2$$

$$\rho_o = \frac{\sin k_x L}{k_x L}$$

$$k_x = \frac{2\pi}{\lambda} (\sin \theta_1 - \sin \theta_2)$$

θ_1 is the angle of incidence

θ_2 is the scattering angle which is measured in the opposite sense from θ_1

L is the length of the surface

T is the correlation length of the surface.

Equation B-25 is limited by the following conditions:

- The surface is perfectly conducting
- Shadowing and multiple scattering may be neglected
- The incident wave is plane and linearly polarized with the E vector either in the plane of incidences, xz, or perpendicular to it
- The observation point is in the far field
- The radius of curvature of the scattering elements is greater than the wavelength of the incident radiation.

The expression for the mean current, which is related to the mean scattered power through Eq. B-4, consists of two terms: (1) a specular term that is a maximum for a smooth surface ($g = 0$) and (2) a diffuse term that is zero for a smooth surface and becomes dominant for a very rough surface ($g > 1$). The specular term is highly directional, as would be expected for the reflection from a smooth surface. Because of conservation of energy, the increase in the specular component as the surface becomes smooth requires a corresponding decrease in the total diffuse component, which causes the speckle. In principal, therefore, a speckly image is always available if the specular component is filtered.

B. SECOND-ORDER STATISTICS

Thus far, this appendix has considered the mean value of the current that related to the average value of the specular and speckle parts. In addition, it is important to determine the fluctuations in these terms. The fluctuations give an indication of the dimensions of the speckle and specular terms. A measure of the fluctuations is obtained from the correlation function of the current.

1. Correlation Expression

The spatial variation in the output current is of interest, since it provides an indication of the fluctuations in the scene and the ability to resolve them. Also, the spatial variation indicates the effect that laser speckle will have on the image. The correlation of the current at two points in the scene is given by

$$\langle i(P_1)\, i(P_2)\rangle = \int R(A)\, \langle I(P_1)\, I(P_2)\rangle\, dA \quad . \qquad \text{(B-26a)}$$

If the spatial mean current is subtracted from the current in order to observe the effect of spatial variations, which provide

information on the speckle, then one obtains

$$\left\langle \left[i(P_1) - \langle i(P_1) \rangle \right] \left[i(P_2) - \langle i(P_2) \rangle \right] \right\rangle = \langle i(P_1) i(P_2) \rangle - \langle i(P_1) \rangle \langle i(P_2) \rangle$$

$$= \int R(A) \left[\langle I(P_1)\, I(P_2) \rangle - \langle I(P_1) \rangle \langle I(P_2) \rangle \right] dA . \qquad \text{(B-26b)}$$

These currents could be obtained simultaneously with two detectors located at the points P_1 and P_2 or with a single detector which is scanned over a time-invariant scene. For a small-size detector, the correlation function of the current would be equal to the correlation of the intensity, since the responsivity could be represented by a delta function.

When the statistics of the surface are Gaussian a simplification can be made, since one has (Ref. B-6)

$$\langle I(P_1)\, I(P_2) \rangle = \langle |E(P_1)|^2 |E(P_2)|^2 \rangle$$

$$= |\langle E(P_1)\, E^*(P_2) \rangle|^2$$

$$+ \langle |E(P_1)|^2 \rangle \langle |E(P_2)|^2 \rangle \qquad \text{(B-27a)}$$

and

$$\langle I(P_1)\, I(P_2) \rangle - \langle I(P_1) \rangle \langle I(P_2) \rangle = |\langle E(P_1)\, E^*(P_2) \rangle|^2 . \qquad \text{(B-27b)}$$

for Gaussian statistics. The correlation function for the intensity is therefore reduced to the evaluation of the correlation of the field and the mean square of the field at each point. For the case where optics are included, the field has been given by Eq. B-11b:

$$\Xi(n) = \frac{e^{i\lambda m^2}}{i\lambda f} \int_y P(y) \left[\int_\xi A(\xi)\, e^{ik_o \left(r_o + \Delta z \cos\theta_2 + \xi \sin\theta_2 - y \sin\theta_2 + \frac{\xi^2 + y^2 - 2y\xi}{2r_o} \right)} e^{i\Delta k r_o} e^{i\phi}\, d\xi \right]$$

$$e^{-i \frac{2\pi}{\lambda f} y\eta}\, dy . \qquad \text{(B-11b)}$$

The correlation function between the points η_1 and η_2 for a scene in the Fresnel region is, therefore,

$$\langle E(\eta_1)\, E^*(\eta_2)\rangle = \int_{\xi_2}\int_{\xi_1} A(\xi_1)\, A^*(\xi_2)\, R(\xi_1,\xi_2)\, T(\xi_1,\xi_2)\, e^{ik_o \sin\theta_2(\xi_1-\xi_2)}\, e^{ik_o \frac{(\xi_1^2-\xi_2^2)}{2r_o}}$$

$$\cdot \int_{y'}\int_{y} P(y)\, P^*(y')\, e^{-ik_o \sin\theta_2(y-y')}\, e^{ik_o \frac{(y^2-y'^2)}{2r_o}}\, e^{-2ik_o \frac{(y\xi_1-y'\xi_2)}{2r_o}}$$

$$e^{-i\frac{2\pi}{\lambda f}(y\eta_1-y'\eta_2)}\, d\xi_1 d\xi_2 dy dy', \qquad \text{(B-28a)}$$

which, in the far field, i.e., where y^2, ξ^2, and ξy variations can be neglected, reduces to

$$\langle E(\eta_1)\, E^*(\eta_2)\rangle = \int_{\xi_2}\int_{\xi_1} A(\xi_1)\, A^*(\xi_2)\, R(\xi_1,\xi_2)\, T(\xi_1,\xi_2)\, e^{ik_o \frac{(\xi_1^2-\xi_2^2)}{2r_o}}\, e^{ik_o \sin\theta_2(\xi_1-\xi_2)}\, d\xi_1 d\xi_2$$

$$\int_{y'}\int_{y} P(y)\, P^*(y')\, e^{-ik_o \sin\theta_2(y-y')}$$

$$\cdot\, e^{-2ik_o \frac{(y\xi_1-y'\xi_2)}{2r_o}}\, e^{-ik_o(\sin\theta_{f1} y + \sin\theta_{f2} y')}\, dy dy' \,. \qquad \text{(B-28b)}$$

The mean square function has been given by Eq. B-12, and the intensity correlation is then given by the sum of the field correlation function and the two mean square field functions as indicated by Eq. B-27.

Equation B-28 can be written as

$$\langle E(P_1) E^*(P_2)\rangle = e^{i\frac{k_o}{2f}(\eta_1^2-\eta_2^2)} \int_{\xi_2}\int_{\xi_1} B(\xi_1,\xi_2)\, e^{ik_o \sin\theta_2(\xi_1-\xi_2)} \int_{y'}\int_{y} Q(y,y')$$

$$e^{-ik_o(\sin\theta_2+\eta_1/f+\xi_1/r_o)y} \cdot e^{ik_o(\sin\theta_2+\eta_2/f+\xi_2/r_o)y'}\, dy dy'\, d\xi_1 d\xi_2 \,,$$

where

$$B(\xi_1,\xi_2) = A(\xi_1)\, A^*(\xi_2)\, R(\xi_1,\xi_2)\, T(\xi_1,\xi_2)\, e^{ik_c \frac{(\xi_1^2-\xi_2^2)}{2r_o}}$$

$$Q(y,y') = P(y)\, P^*(y')\, e^{ik_o \frac{(y^2-y'^2)}{2r_o}} \quad . \tag{B-29}$$

For the far field or Fraunhofer region, the correlation function is the same except that the terms $\exp [ik_o(y^2-y'^2)/2r_o]$ and $\exp (-ik_o\, \xi_1 y/r_o) \exp (ik_o\, \xi_2 y'/r_o)$ are considered to be 1.

The correlation function in the Fresnel region can be rewritten as

$$\langle E(P_1)\, E^*(P_2)\rangle = e^{i\frac{k_o}{2f}(\eta_1^2-\eta_2^2)} \int_{\xi_2}\int_{\xi_1} B(\xi_1,\xi_2) \left[\int_{y'}\int_{y} Q(y,y')\, e^{-ik_o(\sin\theta_2+\eta_1/f+\xi_1/r_o)y} \cdot e^{ik_o(\sin\theta_2+\eta_2/f+\xi_2/r_o)y'}\, dy dy'\right] e^{ik_o \sin\theta_2(\xi_1-\xi_2)}\, d\xi_1 d\xi_2 \ ,$$

$$= e^{i\frac{k_o}{2f}(\eta_1^2-\eta_2^2)} \int_{\xi_2}\int_{\xi_1} B(\xi_1,\xi_2)\, \mathcal{Q}\left[\left(\frac{\sin\theta_2+\eta_1/f+\xi_1/r_o}{\lambda}\right),-\left(\frac{\sin\theta_2+\eta_2/f+\xi_2/r_o}{\lambda}\right)\right] e^{ik_o \sin\theta_2(\xi_1-\xi_2)}\, d\xi_1 d\xi_2$$

where $\mathcal{Q}$ is the Fourier transform of Q. For $\theta_2 = 0$, corresponding to the case where the center of the scene is on the optic axis,

$$\langle E(P_1)E^*(P_2)\rangle = e^{i\frac{k_c}{2f}(\eta_1^2-\eta_2^2)} \int_{\xi_2}\int_{\xi_1} B(\xi_1,\xi_2)\, \mathcal{Q}\left[\left(\frac{\eta_1/f+\xi_1/r_o}{\lambda}\right),-\left(\frac{\eta_2/f+\xi_2/r_o}{\lambda}\right)\right] d\xi_1 d\xi_2 \ , \tag{B-30}$$

where $\mathcal{Q}$ is the Fourier transform of $Q(y,y')$.

Equation B-30 can be recognized as the convolution of the scene characteristics with the statistical spread function, Q. It can be seen that the spread function inverts, in the image plane, the location of a point in the object plane and demagnifies it by the factor f/r. In the far field, however, the term Q can be taken outside the integral.

From these equations, it can be seen that Eq. B-30 is a convolution integral on the right side, so that

$$\langle E(P_1)E^*(P_2)\rangle = B(\eta_1,\eta_2) * Q(\eta_1,\eta_2)$$

$$Q(\eta_1,\eta_2) * B(\eta_1,\eta_2) \quad . \qquad \text{(B-31)}$$

This equation can be compared with the response of a nonstatistical coherent system in which

$$I(P_1) = |h * E_s|^2 \qquad \text{(B-32)}$$

and an incoherent system in which

$$I(P_1) = |h|^2 * |E_s|^2 \quad . \qquad \text{(B-33)}$$

2. Roughness Considerations

The spatial variation of the current is found by substituting values from the correlation equations into Eq. B-27. Equation B-27 can then be used to determine the effect of speckle on the image.

If the scene information and the turbulence effects are again ignored, the effect of roughness in the focal plane for the far-field case is determined from Eq. B-28b to be

$$\langle E(y)\, E^*(y')\rangle = \int_{\xi_2}\int_{\xi_1} R(\xi_1,\xi_2)\, e^{ik_o \sin\theta_2(\xi_1-\xi_2)}\, d\xi_1 d\xi_2 \quad , \qquad \text{(B-34)}$$

and the second-order equation corresponding to Eq. B-15 is

$$\langle \rho(y)\, \rho^*(y') \rangle = \frac{F'_2 F^*_2}{4L^2} \int_{-L}^{L}\int \chi_2 \, (k_{z1}, - k_{z2}) \, e^{i(k_{x1}\xi_1 - k_{x2}\xi_2)} \, d\xi_1 d\xi_2 \quad . \quad \text{(B-35)}$$

When Eq. B-21 is substituted into Eq. B-35, one obtains

$$\langle \rho(y)\rho^*(y') \rangle = K' \int_{-L}^{L} e^{\frac{-m}{T^2}\xi_2^2} e^{-ik_{x2}\xi_2} \int_{-L}^{L} e^{\frac{-m}{T^2}\xi_1^2} e^{i(k_{x1} - \frac{2mi}{T^2}\xi_2)\xi_1} \, d\xi_1 \, d\xi_2 \quad ,$$

where

$$k' = \frac{F'_2 F^*_2}{4L^2} \, e^{\frac{-\sigma}{2}(k_{z1}^2 + k_{z2}^2)} \sum_{m=o}^{\infty} \frac{\sigma^{2m} \, k_{z1}^m \, k_{z2}^m}{m!} \quad .$$

When the same procedure as from Eq. B-23 to Eq. B-25 is followed, the result is

$$\langle \rho(y) \, \rho^*(y') \rangle = F'_2 F^*_2 \, e^{\frac{-\sigma^2}{2}(k_{z1}^2 + k_{z2}^2)} \left[\frac{\sin k_{x1} L}{k_{x1} L} \, \frac{\sin k_{x2} L}{k_{x2} L} \right.$$

$$\left. + \frac{\sqrt{\pi}\, T}{L} \, \frac{\sin (k_{x2} - k_{x1}) L}{(k_{x2} - k_{x1}) L} \sum_{m=1}^{\infty} \frac{\sigma^{2m} \, k_{z1}^m \, k_{z2}^m}{m! \, \sqrt{m}} \, e^{\frac{-T^2 k_{x2}^2}{4m}} \right] \quad . \quad \text{(B-36)}$$

Substitution of Eq. B-36 into Eq. B-27b yields

$$|\langle E(P_1)\, E^*(P_2)\rangle|^2 = |F_2\, F'_2|^2\, e^{-\sigma^2(k_{z1}^2 + k_{z2}^2)} \left[\frac{\sin^2 k_{x1} L}{(k_{x1} L)^2} \frac{\sin^2 k_{x2} L}{(k_{x2} L)^2} \right.$$

$$+ \frac{2\sqrt{\pi}\, T}{L} \frac{\sin(k_{x2}-k_{x1})L}{(k_{x2}-k_{x1})L} \frac{\sin k_{x1} L}{k_{x1} L} \frac{\sin k_{x2} L}{k_{x2} L} \sum_{m=1}^{\infty} \frac{\sigma^{2m} k_{z1}^m k_{z2}^m}{m!\ \sqrt{m}} e^{\frac{-T^2 k_{x2}^2}{4m}}$$

$$\left. + \frac{\sqrt{\pi} T}{L} \frac{\sin^2(k_{x2}-k_{x1})L}{[(k_{x2}-k_{x1}L]^2} \left| \sum_{m=1}^{\infty} \frac{\sigma^{2m} k_{z1}^m k_{z2}^m}{m!\ \sqrt{m}} e^{\frac{-T^2 k_{x2}^2}{4m}} \right|^2 \right] . \quad \text{(B-37)}$$

Equation B-37 consists of a term that is exclusively due to the speckle component and a term that is exclusively due to the specular component. It also contains a cross-product term that depends on both the speckle and specular effects. Again, a specular term that is relatively constant is obtained plus a speckle term that is a function of the roughness and the correlation length. In the limit when the correlation length is zero, the spot size is obtained corresponding to the Airy disc which is simply due to the specular term. This interpretation of the result for zero correlation length is considerably different from the interpretation made by Goodman (Ref. B-7) in his analysis of the zero-correlation-length problem, in which the results are considered analogous to the Van Cittert-Zernicke theorem.

REFERENCES, APPENDIX B

B-1. V. J. Corcoran, "Directional Processes in Optical Heterodyne Detection Processes," *Jour. Appl. Phys.*, Vol. *36*, 1965, p. 1819.

B-2. M. Born and E. Wolf, *Principles of Optics*, Macmillan Company, New York, 1959, p. 381.

B-3. J. W. Goodman, *Introduction to Fourier Optics*, McGraw-Hill Book Company, New York, 1968, p.78.

B-4. *Ibid*, p. 90.

B-5. P. Beckmann and A. Spizzichino, *The Scattering of Electromagnetic Waves from Rough Surfaces*, Pergamon Press, New York, 1963, pp. 70-98.

B-6. I. S. Read, "On a Moment Theorem for Complex Gaussian Processes,: *IRE Trans. Information Theory*, Vol. IT-8, 1962, p. 194.

B-7. J. W. Goodman, "Statistical Properties of Speckle Patterns," in J. C. Dainty, ed., *Laser Speckle and Related Phenomena*, Vol. *9* of *Topics in Applied Physics*, Springer-Verlag, Berlin Heidelberg, 1975, pp. 9-75.

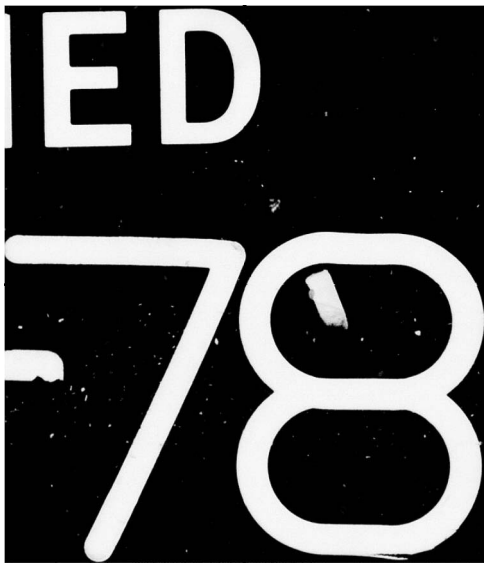
ED
78